

# Antisymmetrization in the Multicluster Dynamic Model of Nuclei and the Nucleon Exchange Effects

R.A. Eramzhyan<sup>1,2</sup>, G.G. Ryzhikh<sup>1,3</sup>, and Yu.M. Tchuvil'sky<sup>4</sup>

<sup>1</sup> Institute for Nuclear Research of the Russian Academy of Sciences, Moscow 117312, Russia

<sup>2</sup> Cyclotron Institute, Texas A&M University, College Station, TX 77843-3366, USA

<sup>3</sup> Faculty of Science, Northern Territory University, Darwin NT 0909, Australia

<sup>4</sup> Institute of Nuclear Physics of Moscow State University, Moscow 119899, Russia

## Abstract

A modified version of the Multicluster Dynamic Model of nuclei is proposed to construct completely antisymmetrized wave functions of multicluster systems. An overlap kernel operator is introduced to renormalize the total wave function after antisymmetrization between nucleons in different clusters. A group-theoretical method is developed to analyze the role of the exchange effects arising in the calculation of the various observables of multicluster systems due to this antisymmetrization.

The Antisymmetrized version of the Multicluster Dynamic Model is applied to the six-nucleon systems treating them as  $\alpha$ -2N ones. The static and dynamic characteristics of the six-nucleon systems manifested in electron and  $\pi$ -meson scattering, muon capture,  $\beta$ -decay, pion photoproduction, etc., are calculated. Significant progress is achieved in describing of variety of dynamic observables of the six-nucleon systems as compared to the multicluster dynamic model. In most cases calculated static and especially dynamic characteristics are in a good agreement with the experimental data.

*Keywords:* nuclear structure, nuclear models, light nuclei, nuclear reactions, electron scattering, pion scattering, pion photoproduction, muon capture.

PACS numbers: 21.60.Gx, 27.20.+n, 25.30.-c, 25.80.-e

## I. INTRODUCTION

To describe the structure of light nuclei ( $A > 4$ ) in great detail very sophisticated approaches are now being elaborated. Recently, Green's Function Monte Carlo calculations have been realized [1] for nuclei with  $A \leq 6$  starting from the realistic nucleon-nucleon interaction. At the same time the stochastic variational method (this method was first applied in calculations of nuclear structure within the multicluster dynamic model (MDM) in Ref. [2]) has been extended to the systems with  $A \leq 10$  treating all nucleons variables on the same ground (see, for example, Ref. [3]). Before that the K-harmonic method [4,5] and the extended shell model [6,7] have been used to learn more about the structure of the 1p-shell nuclei. However, practical applications of all these methods is not an easy task. That is why there are not many observables analyzed with these newly developed methods. For this reason they are unable to displace the traditional approaches, considering the fact that the latter are improved as well.

The Microscopic Cluster Model (MCM) still continues to play a role as a very successful approach well suited for description of the structure of light nuclei. This model in its development has passed many stages, starting from its simplest realization within the framework of the single channel Resonating Group Method (RGM) [8] and coming finally to the many-channel multicluster MCM [9–11,3].

This model proceeds from the tendency of the nucleons to form clusters inside the light nuclei due to their strong binding. In the MCM the  $A$ -nucleon wave function is approximated by a superposition of the antisymmetrized basis functions in which nucleons have been grouped into some clusters —  $\alpha$ ,  ${}^3\text{He}$ ,  ${}^3\text{H}$ ,  $d$  etc. The cluster internal wave functions are supposed to be known from the beginning but the relative motion function is obtained from the solution of the dynamic equation (or also from the system of coupled equations) derived straightforwardly from the initial  $A$ -nucleon problem.

This approach in its final version enables us to incorporate into the calculation various multicluster configurations, to take into account some effects of the cluster excitations and their rearrangement, to treat nucleons on the same ground as clusters, etc. Finally a consistent and successful description of bound, resonant and scattering states of many nuclei [9–12] has been

achieved.

At the same time extensive applications of the MCM have revealed some deficiencies which show up mainly in the case when the short-range correlations among nucleons appear to be important. Refined realization of the model requires that more realistic nucleon-nucleon interaction should be used and, consistently, more realistic wave functions of clusters should be involved in the calculation. But such a program is extremely difficult to realize in practice. Indeed the cluster-cluster potential which finally arises in the MCM comes about from the folding of the NN potential over the intrinsic wave functions of the constituent clusters. This potential appears to be very complicated, highly nonlocal and energy dependent due to the exchange effects and the composite nature of clusters. If one starts from the cluster internal wave functions with both short range and tensor NN correlations and uses the realistic NN forces with the noncentral components, then one arrives to such a complicated cluster-cluster potential that it becomes almost useless for practical applications. That is why a simple intrinsic wave function of cluster and a simplified effective NN forces are usually used in practice. Of course in this case this approach loses its "pure" microscopic character and it becomes model dependent.

On the other hand, when one starts from the NN potential with a strong short-range repulsion and uses noncorrelated wave functions of clusters then the results of the calculation become highly dependent on the number and the type of the cluster channels taken into account [13,14]. In spite of this fact, many calculations are still undertaken in this approximation with forces like the Hasegawa-Nagata or the Eikemeier-Hackenbroich one (see, for example, Refs. [15,16]).

There is another problem which is a principal one for the MCM. Derived from the more or less realistic NN potential, the cluster-cluster potential of the MCM does not reproduce accurately the phase shifts for free clusters. This problem was studied thoroughly in the case of the simplest cluster system, namely for the  $\alpha$ -N (see Ref. [17]). Here the N- $\alpha$  potential was constructed starting from a realistic NN potential and a very complicated  $\alpha$ -particle wave function. It turned out that even in this simple case, in order to reproduce the experimental  $\alpha$ -N phase-shifts the starting realistic nucleon-nucleon potential had to be modified significantly. It means that in the MCM, a phenomenological (effective) NN-potentials should be used rather than the realistic ones.

At the same time a microscopically inspired Potential Cluster Model, which is also called the Multicluster Dynamic Model — MDM, has been also applied successfully for the calculation of the structure of light nuclei. Formulation of the MDM is given, for example, in Ref. [18]. In this approach the relative motion function of clusters is obtained as a solution of the  $k$ -cluster dynamic equations with the cluster-cluster potentials derived directly from the phase-shifts analysis. Thus, in the MDM the on-shell behavior of the interaction amplitudes are taken from the outset with higher precision as compared to the MCM.

In the MDM there is no problem at all with the intrinsic cluster wave functions due to the factorization of the matrix elements squared for the nuclear observables. Due to this factorization, it is not the intrinsic cluster wave functions but rather the magnitudes of their observables (that are directly taken from experiments) which are used here. In this way many observables of the clusterized nuclei were obtained in a good agreement with the experimental data (see, for example, Refs. [19–21]). Another attractive point of the MDM is its much more simple formalism as compared to the MCM. These simplifications come from the approximate treatment of the Pauli-principle for the nucleons from different clusters.

However, there are some observables where just the nucleon exchanges between different clusters are of primary importance. That is why we have modified the MDM to construct finally completely antisymmetrized wave functions. This modified version of the model was called the AMDM — the Antisymmetrized version of the MDM. It was shown in Ref. [22] that by using the AMDM we extend the list of well reproduced observables as compared to the MDM. In particular, it was possible to describe all longitudinal and transversal elastic and inelastic electromagnetic form factors of  ${}^6\text{Li}$  simultaneously for a broad interval of the momentum transfer. At the same time the AMDM formalism is still more simple and transparent than the MCM one.

The method of construction of the totally antisymmetric wave function from the MDM function which had been used in our earlier works [22,23] has some limitations. The fact is that after antisymmetrization of the MDM functions between nucleons from the different clusters, the set of total wave functions obtained loses the orthonormalization property. First of all one has to restore the total normalization of the wave functions. In Ref. [23] it was done by the simplest way of multiplying the wave function by a constant. This is a common procedure for the shell model

approach where the number of oscillator quanta for each wave function is fixed. However, in general case such a procedure is not quite correct. The reason is that the constant renormalization ( $C$ -renormalization as we will abbreviate it further) does not restore the orthogonality between different antisymmetrized wave functions with the same total quantum numbers. Moreover, this  $C$ -renormalization changes the asymptotic part of the relative motion wave function where the antisymmetrization must have no influence at all.

Experience accumulated in the MCM suggests that the renormalization with the integral exchange kernel ( $K$ -renormalization), which appears primarily in the RGM, will allow us to solve this problem in the general case as well. It is very important that there is a kernel renormalization that allows to determine the class of observables which are exactly conserved under the antisymmetrization [24]. Some aspects of the renormalization problem have been discussed already in Ref. [25] for  ${}^6\text{Li}$  which was treated as a three-cluster system. In this paper we present new precisely renormalized version of the AMDM and its application to many observables of the six-nucleon systems. The six-nucleon system is particularly singled out in nuclear physics and has been studied in many papers as a three-nucleon system. Six nucleons in nuclei exhibit quite properly the typical properties of all light nuclei, such as the decisive role of the Pauli principle, the substantial spin-orbit splitting of levels, a significant greater role of the interaction of valent nucleons with core compared with the interaction among them, the important contribution of the short-range correlations of nucleons, etc. These circumstances, as well as numerous experimental data obtained for six-nucleon systems including the strong, electromagnetic and weak interaction processes permit their theoretical studies to be regarded as a theoretical laboratory for nuclear physics in a broad sense allowing to test new theoretical approaches.

This paper is organized in the following way. In Section II the formalism of the AMDM is briefly described and a group-theoretical analysis of matrix elements for various observables is performed. In Section III many observables of the  $A=6$  nuclei treated as a three-cluster  $\alpha$ -2N systems are analyzed within the framework of both versions of the AMDM — with constant and kernel renormalization. All these results are compared to those obtained within the MDM. Besides the traditional observables — static properties of ground state, beta-decay and electron scattering — we are discussing muon capture, pion scattering and pion photoproduction. All

these reactions proceed via similar nuclear transition operators. Studying all of these transitions does not simply lead to a large amount of redundant information, but, rather, it generally leads to complementary information. So the most informative approach for studying the nuclear structure is to carry out a simultaneous study of all of them. We conclude in Section IV.

## II. GENERAL PROPERTIES OF THE AMDM

### A. Construction of the MDM wave function

The AMDM is essentially based on the MDM. Therefore it makes sense to run briefly through the basic ingredients of the MDM.

Let  $A$  identical fermions (nucleons in our case, but they could be quarks, etc.) be distributed over  $k < A$  clusters. Individual nonclusterized (valent) fermions, if they appear in this case, are treated as clusters as well.

In the MDM, for a system made up of the  $k$  clusters the wave function, with given total momentum  $J$ , total isospin  $T$  and their projections  $M$  and  $M_T$ , is defined as

$$\Psi_{JM}^{\text{MDM}}(\{\vec{\xi}^{\text{tot}}\}) = \sum_{\{\vec{\ell}\}\{\vec{j}\}\{l\}} \left\{ \left\{ \Phi^{\text{int}} \right\}_{TM_T, J_c M_c}^k, \Psi_{LM_L}(\{\vec{\xi}\}) \right\}_{JM}, \quad (1)$$

where  $J_c$  is the channel spin,  $\{\vec{\xi}^{\text{tot}}\}$  denotes the complete set of the intercluster Jacoby coordinates.  $\Psi_{LM_L}(\{\vec{\xi}\})$  is the function of the cluster-cluster relative motion with the total angular momentum  $L$ . It depends on the corresponding set of the Jacoby coordinates  $\{\vec{\xi}\}$ . Each coordinate  $\vec{\xi}_j$  is divided into angular and spatial parts:  $\vec{\xi}_j = (\hat{\xi}_j, \xi_j)$ .

We first define some notations to be used in this Section. Let's  $x$  to be any momentum ( $l$  — angular momentum,  $s$  — spin,  $\vec{j} = \vec{l} + \vec{s}$  — total momentum,  $t$  — isospin) and  $m_x$  its projection, then the symbol  $\{\dots\}_{x m_x}^k$  will denote the coupling scheme of the individual momenta  $x_i$  and their projections  $m_{x_i}$  to the intermediate  $x_{12}, \dots, x_{12\dots k}$  momenta and the total,  $x$ , momentum and its projection:

$$\{\dots\}_{x m_x}^k = \{ \{ \{ \{ x_1 x_2 \}_{x_{12}} x_3 \}_{x_{123}} \dots x_k \}_{x m_x} \}. \quad (2)$$

Correspondingly, the symbol with double down index is defined as:

$$\{\dots\}_{xm_x, ym_y}^k = \{\dots\}_{xm_x}^k \{\dots\}_{ym_y}^k . \quad (3)$$

The following abbreviations are used to list the intermediate momenta in eq. (1):

$$\begin{aligned} \{\tilde{j}\} &= (j_{12}, j_{123}, \dots, j_{12\dots k}, J_c), \\ \{\tilde{t}\} &= (t_{12}, t_{123}, \dots, t_{12\dots k}, T), \\ \{l\} &= (l_1, l_2, \dots, l_{k-1}, l_{12}, l_{123}, \dots, l_{12\dots k-1}, L), \end{aligned} \quad (4)$$

where  $l_i$  is the orbital momentum conjugated with the  $i$ -th Jacoby coordinate of the relative motion;  $L$  is the total angular momentum of the system,  $J_c$  is the spin of the channel. The total momentum  $J$  equals to the sum  $\vec{J} = \vec{J}_c + \vec{L}$ . Finally the complete set of quantum numbers  $\{\omega\}$  which characterizes any channel of the system is defined as

$$\{\omega\} = (\{\tilde{j}\}, \{\tilde{t}\}, \{l\}, J). \quad (5)$$

According to the MDM, the internal wave function of the clusters  $\Phi^{int}$  is not modified in the nucleus and it is built up from the wave functions of free clusters in their ground states:

$$\Phi^{int} = \prod_{i=1}^k \phi_{j_i m_i, t_i m_{t_i}}^i(\{\tilde{\xi}_i^{int}\}), \quad (6)$$

where  $\{\tilde{\xi}_i^{int}\}$  is the set of the internal Jacoby coordinates for the  $i$ -th cluster and  $j_i$  and  $t_i$  are their total momentum and isospin with projections  $m_i$  and  $m_{t_i}$ , respectively. The role of the cluster polarization inside a nucleus has been studied recently within the MCM. It was shown in Refs. [13,14] that the  $\alpha$ -cluster is polarized very weakly inside light nuclei. Therefore, the assumption that the  $\alpha$ -cluster can be considered as a free  $\alpha$ -particle is rather good in any multicluster approach.

The wave function of the cluster-cluster relative motion  $\Psi_{LM_L}(\{\vec{\xi}\})$  is decomposed into the angular  $Y_{\{l\}M_l}(\hat{\xi})$  and the radial  $F_{\{\omega\}}(\xi)$  parts. The angular part of the relative wave function can be written as:

$$Y_{\{l\}M_l}(\hat{\xi}) = \left\{ \prod_{i=1}^{k-1} Y_{l_i m_{l_i}}(\hat{\xi}_i) \right\}_{LM_L}^{k-1}. \quad (7)$$

It is very convenient to present the radial wave function of the relative motion in terms of the superposition of gaussians (it was demonstrated in many papers, see for example Ref. [19]) as follows:



$$F_{\{\omega\}}(\xi) = \sum_{\nu} C_{\nu}^{\{\omega\}} \prod_{i=1}^{k-1} |\xi_i|^{l_i} \exp(-\alpha_{\nu i}^{\{\omega\}} \xi_i^2), \quad (8)$$

where  $C_{\nu}^{\{\omega\}}$  and  $\alpha_{\nu i}^{\{\omega\}}$  are the expansion coefficients. The set of these coefficients together with the set of the "channel" quantum numbers  $\{\omega\}$  determine completely the MDM wave function. The variational method for solution of the  $k$ -cluster problem is well suited for finding these coefficients. As it was shown in Refs. [19,20], such an approach allows to obtain a very accurate solution of the nuclear few-body problem. It is the gaussian parameterization of the MDM wave function that makes it possible to get analytical expression for most matrix elements both in the MDM and in the AMDM (see, for example, Refs. [22,23,26]).

As it was shown by Saito [27] that sophisticated nonlocal energy-dependent "microscopic" cluster-cluster forces appearing in the RGM can be successfully approximated by a simple local  $E$ -independent ones if they are supplemented by the orthogonality requirement based on the Pauli principle. In such an approach, both the phase shifts and the nodal structure of the RGM wave functions can be quite well described in a very simple way. This is the basic approximation for the Orthogonality Condition Model (OCM) [27,28] and, in fact, for any MDM. In the version of the MDM [19] to be used throughout this paper, the Pauli-forbidden components are excluded from the solution of the MDM dynamic equations by means of the pseudopotential technique [19,29]. As we already stated before, such "microscopically inspired" intercluster forces have even some advantage compared to the "true microscopic" ones. This advantage consists in more accurate description of the low-energy cluster-cluster phase shifts and, therefore, the most important on-shell properties of the cluster-cluster forces.

However, exclusion solely of the forbidden components does not account for all the consequences of the Pauli principle for the multicluster system. Exchanges between nucleons in the different clusters are completely omitted in the MDM. That is why some types of observables can not be explained in the framework of this model. Therefore we came to recognize that the totally Antisymmetrized MDM (the AMDM) should be used in general case [22,23]. Notice that the AMDM is, in fact, a modification and generalization of the OCM.

## B. Wave functions of the AMDM

In the initial version of the AMDM [22] named here as AMDM<sub>C</sub> the total wave function was constructed by means of direct antisymmetrization of the MDM wave function:

$$\Psi_A = \frac{1}{Q} \hat{A} \Psi^{MDM} . \quad (9)$$

As we have noted above, in this case we use a constant  $Q$  to normalize the total function  $\Psi_A$ . That is why we call this version of the model as the AMDM<sub>C</sub> — Antisymmetrized Multicluster Dynamic Model with the renormalization to the constant.  $\hat{A}$  in eq.(9) is an antisymmetrizer:

$$\hat{A} = \Omega^{-1} \left( 1 + \sum_P (-1)^p \hat{P} \right) , \quad (10)$$

where the normalizing factor  $\Omega$  has the following form:

$$\Omega = \left( \frac{A!}{\prod_{i=1}^k A_i!} \right)^{\frac{1}{2}} . \quad (11)$$

Here  $A_i$  is the mass of the individual cluster  $i$ ,  $\hat{P}$  is the operator permutating nucleons between different clusters and  $p$  is the parity of such a permutation.

In a new version of the AMDM, named the AMDM<sub>K</sub>, the overlap kernel operator  $\hat{K}$  is introduced to renormalize the total wave function after antisymmetrization:

$$\Psi_A = \hat{A} \sum_{\{\hat{i}\}\{\hat{j}\}\{\hat{l}\}} \left\{ \left\{ \Phi^{int} \right\}_{TM_T, J_c M_c}^k \cdot \hat{K}^{-1/2} \Psi_{LM_L}(\{\hat{\xi}\}) \right\}_{JM} . \quad (12)$$

This operator  $\hat{K}$  acts in the Hilbert space of the  $(3k - 3)$ -dimensional orbital functions of the  $k$ -cluster system (cluster subspace). It acts on the function in the following way:

$$\hat{K} \Psi(\{\vec{\xi}^l\}) = \int d\{\vec{\xi}^n\} K(\{\vec{\xi}^l, \vec{\xi}^n\}) \Psi(\{\vec{\xi}^n\}) . \quad (13)$$

The overlap kernel  $K(\{\vec{\xi}^l, \vec{\xi}^n\})$  is defined as a projection of the antisymmetrizer onto the cluster subspace of  $A$ -nucleon variables:

$$K(\{\vec{\xi}^l, \vec{\xi}^n\}) = \Omega \cdot \left\langle \left\{ \Phi^{int} \right\}_{S,T}^k \prod_{i=1}^{k-1} \delta(\vec{\xi}_i - \vec{\xi}_i^l) \mid \hat{A} \mid \left\{ \Phi^{int} \right\}_{S,T}^k \prod_{i=1}^{k-1} \delta(\vec{\xi}_i - \vec{\xi}_i^n) \right\rangle . \quad (14)$$

The eigenfunctions  $\Phi_\nu(\{\vec{\xi}\})$  and the eigenvalues  $\varepsilon_\nu$  of this kernel satisfy the usual equation:

$$\hat{K}\Phi_\nu(\{\vec{\xi}\}) = \varepsilon_\nu\Phi_\nu(\{\vec{\xi}\}), \quad (15)$$

and

$$\hat{K}^{-1/2}\Phi_\nu(\{\vec{\xi}\}) = \varepsilon_\nu^{-1/2}\Phi_\nu(\{\vec{\xi}\}), \quad (16)$$

for

$$\varepsilon_\nu \neq 0. \quad (17)$$

In the MDM, any nucleus is usually considered as a system composed of some number of magic clusters ( $\alpha$ -particles,  $^{16}\text{O}$ , etc.) in their ground states and  $n$ -valent nucleons. In this Section, to make the group-theoretical analysis more transparent we restrict the general case by the following two conditions:

1. The magic clusters are considered to be the SU(3) and SU(4) scalars. So, in their wave functions we neglect all components violating these symmetries. If the system is built up from different clusters ( $\alpha$ -particles and  $^{16}\text{O}$ , for example) we will neglect also the difference in their oscillator parameters  $\hbar\omega$  in order to conserve the SU(3) scalar character of  $\{\Phi^{int}\}_{S,T}^k$ .
2. The valent group of  $n$  nucleons is considered either as one light cluster with three or less nucleons (with the common oscillator parameter  $\omega$ ) or as nonclusterized nucleonic system if  $n \leq 2$ .

These conditions lead to that the total spin  $S = J_c$  and isospin  $T$  are uniquely determined by the Young scheme [f] and Yamanouchi symbol ( $r$ ). These quantum numbers are precisely those that characterize the MDM functions.

As a consequence of the SU(3)-symmetry, the eigenfunctions of the operator  $\hat{K}$  are the many-body oscillator functions with a definite number of oscillator quanta  $N$  and a fixed value of the Elliott symbols  $(\lambda\mu)$ . Since the same Elliott symbol can characterize several eigenfunctions, an additional quantum number  $i$  is introduced to distinguish among them. The eigenfunctions of the operator  $\hat{K}$  are characterized by the total angular momentum  $L$ . It is interesting to note that its eigenvalues do not depend on  $L$  at all. Finally for a complete definition of eq.(15) we specify a symbol  $\nu$  as:

$$\nu = (S, T, L, N, (\lambda\mu), i). \quad (18)$$

According to these restrictions the internal part of the MDM function can be written down in the factorized form:

$$\left\{ \Phi^{int} \right\}_{J_c M_c, T M_T}^k = \Phi_{int} \cdot \left\{ \prod_{i=1}^k \chi_{s_i t_i} \right\}_{S M_S, T M_T}^k, \quad (19)$$

where  $\Phi_{int}$  is a scalar spatial function and the rest is the spin-isospin one. To simplify the reading of the subsequent equations we will use the following notations for the spin-isospin function:

$$\chi_{ST} = \chi_{[f](r)} = \left\{ \prod_{i=1}^k \chi_{s_i t_i} \right\}_{S M_S, T M_T}^k. \quad (20)$$

Before concluding this subsection we note that these restrictions are used only in Section II for the sake of the formal analysis of the antisymmetrization effects. As to the numerical calculations in Section II, more complicated wave functions were actually used. On the other hand, it appeared that the results of the formal analysis are valid even in the case when the conditions 1 and 2 are not fulfilled exactly.

### C. Formal analysis of the matrix elements within the framework of the AMDM

Before starting any discussion of the results of the calculations within the framework of the AMDM it is very instructive to make some classification of the nuclear matrix elements. For this reason let us expand the relative motion functions of the MDM onto the eigenfunctions  $\Phi_\nu$  of the overlap kernel:

$$\Psi(\{\vec{\xi}\}) = \sum_{\nu} b_{\nu} \Phi_{\nu}(\{\vec{\xi}\}). \quad (21)$$

Generally, the wave function in the multicluster approach can contain some admixture of the Pauli-forbidden components with  $\varepsilon_{\nu} = 0$ . After antisymmetrization these components have to disappear. To simplify the subsequent expressions, it is assumed below that such forbidden components have been eliminated from the beginning (i.e.  $b_{\nu} = 0$  if  $\varepsilon_{\nu} = 0$ ). So one can write down that:

$$\langle \Phi | \hat{O} | \Phi' \rangle = \sum_{\nu_1 \nu_2} b_{\nu_1} b_{\nu_2} \varepsilon_{\nu_1}^{-\frac{1}{2}} \varepsilon_{\nu_2}^{-\frac{1}{2}}.$$

$$\langle \hat{A} \{ \Phi_{int} \Phi_{\nu_1}(\{\vec{\xi}_i\}) \chi_{[f](r)} \} | \hat{O} | \hat{A} \{ \Phi_{int} \Phi_{\nu_2}(\{\vec{\xi}_i\}) \chi'_{[f'](r')} \} \rangle. \quad (22)$$

For any operator  $\hat{O}$  which is symmetric over the nucleon permutations one can replace an antisymmetrizer, say in the left hand side of eq. (22), by the factor  $\Omega$ . Let us then add to this expression the sum over the complete set of the nonantisymmetrized wave functions:

$$1 = \sum_{(j)\nu[f''](r'')} | \Phi_{int}^{(j)} \Phi_{\nu}(\{\vec{\xi}_i\}) \chi_{[f''](r'')} \rangle \langle \Phi_{int}^{(j)} \Phi_{\nu}(\{\vec{\xi}_i\}) \chi_{[f''](r'')} \rangle, \quad (23)$$

where the sum over  $(j)$  includes all orbital excitations of the constituent clusters. Because the antisymmetrizer does not change the values of the total spin  $S$ , isospin  $T$  and Young scheme  $[f]$  of the system one arrives to the following expression for the matrix elements:

$$\begin{aligned} \langle \Phi | \hat{O} | \Phi' \rangle = \Omega \sum_{\nu_1 \nu_2 \nu(j)\nu(r'')} b_{\nu_1} b_{\nu_2} \varepsilon_{\nu_1}^{-\frac{1}{2}} \varepsilon_{\nu_2}^{-\frac{1}{2}} \langle \Phi_{int}^{(0)} \Phi_{\nu_1}(\{\vec{\xi}_i\}) \chi_{[f](r)} | \hat{O} | \Phi_{int}^{(j)} \Phi_{\nu}(\{\vec{\xi}_i\}) \chi''_{[f'](r'')} \rangle \cdot \\ \langle \Phi_{int}^{(j)} \Phi_{\nu}(\{\vec{\xi}_i\}) \chi''_{[f'](r'')} | \hat{A} | \Phi_{int}^{(0)} \Phi_{\nu_2}(\{\vec{\xi}_i\}) \chi'_{[f'](r')} \rangle. \end{aligned} \quad (24)$$

Here the index  $(j) = (0)$  labels the intrinsic orbital functions of clusters in their ground states.

From eq. (24) it follows that if the operator  $\hat{O}$  is diagonal in the space of the orbital functions  $\Phi_{int}^{(j)} \Phi_{\nu}(\{\vec{\xi}_i\})$  and over the Yamanouchi symbols  $(r)$  then the matrix elements of the MDM and AMDM are equal to each other because in this case  $(j) = (0)$  only and according to expressions (12), (14) and (15) the matrix element of the antisymmetrizer reduces to  $\varepsilon_{\nu_2} \delta_{\nu\nu_2}$ . Such a situation occurs when:

1. An operator is of pure spin-isospin type.
2. An operator is of particular spatial type being a function of the Casimir operators of the  $SU(3)$  group and its subgroups.

Indeed in the last case this operator is diagonal because the wave functions in (24) have a definite  $SU(3)$  symmetry, and the Elliott symbol  $(\lambda\mu)$  is a good quantum number for the system.

It is interesting to analyze the difference between the matrix elements of the full tensor operators and the matrix elements of the pure spatial ones. For this purpose let us use the following representation of the wave function:

$$\hat{A} | \Phi_{int}^{(0)} \Phi_{\nu_2}(\{\vec{\xi}_i\}) \chi_{[f](r)} \rangle = \frac{\Omega}{n_f} \sum_r \hat{C}_{rr}^{[f]} | \Phi_{int}^{(0)} \Phi_{\nu_2} \chi_{[f](r)} \rangle, \quad (25)$$

where  $\hat{C}_{rr}^{[f]}$  is the Young operator which projects the wave function onto the wave function with the definite Young scheme  $[f]$  and Yamanouchi symbol  $(r)$  ( $n_f$  is a dimension of the corresponding representation):

$$\hat{C}_{rr}^{[f]} = \frac{n_f}{A!} \sum_P D_{rr}^{[f]}(P) \hat{P}. \quad (26)$$

Here  $D_{rr}^{[f]}(P)$  is the matrix of the corresponding representation of the permutation group.

After substitution of eq. (25) into eq. (24), one arrives at the following expression:

$$\begin{aligned} \langle \Phi | \hat{O} | \Phi' \rangle &= \sum_{\nu_1 \nu_2 \nu(j)(r)} b_{\nu_1} b_{\nu_2} \langle \Phi_{int}^{(0)} \Phi_{\nu_1}(\{\vec{\xi}_i\}) \chi_{[f](r_0)} | \hat{O} | \Phi_{int}^{(j)} \Phi_{\nu}(\{\vec{\xi}_i\}) \chi'_{[f'](r)} \rangle \\ &Q_{\nu_1}^{-1} Q_{\nu_2}^{-1} \langle \Phi_{int}^{(j)} \Phi_{\nu}(\{\vec{\xi}_i\}) | \hat{C}_{rr}^{[f']} | \Phi_{int}^{(0)} \Phi_{\nu_2}(\{\vec{\xi}_i\}) \rangle, \end{aligned} \quad (27)$$

where

$$Q_{\nu} = \langle \Phi_{int}^{(0)} \Phi_{\nu}(\{\vec{\xi}_i\}) | \hat{C}_{rr}^{[f']} | \Phi_{int}^{(0)} \Phi_{\nu}(\{\vec{\xi}_i\}) \rangle^{\frac{1}{2}} = \Omega^{-1} (n_f \varepsilon_{\nu})^{\frac{1}{2}}. \quad (28)$$

$Q_{\nu}$  is the normalization factor of the wave function  $C_{rr}^{[f']} | \Phi_{int}^{(0)} \Phi_{\nu}(\{\vec{\xi}_i\}) \rangle$ .

Now we are ready to establish some relation between the renormalization factor  $Q$  in eq.(9), which have appeared in the AMDM<sub>C</sub> and the eigenvalues of the overlap kernel  $\varepsilon_{\nu}$ :

$$Q^2 = \frac{n_f}{\Omega} \sum_{\nu} (b_{\nu})^2 \varepsilon_{\nu}, \quad (29)$$

Let us compare now matrix elements of a pure spatial operator with matrix elements of a full tensor one. It follows from eq. (9) that in the latter case only the terms with the Yamanouchi symbols  $(r) \neq (r_0)$  contribute to the AMDM matrix element, contrary to the case of a pure spatial operator. Evidently such terms are not present in the MDM case independently of the tensor structure of any operator. That is why the matrix elements of a full tensor operator are expected to be modified much more than the matrix elements of a pure spatial one when the exchange terms are taken into account.

Eq.(27) allows to establish some properties of matrix elements appearing in various reactions as well. To demonstrate this let us consider, for example, the cluster knock out reaction at large

momentum transfer, though it is beyond the scope of this paper. Nevertheless, it is instructive to say some words about this case. The amplitude of the corresponding process is proportional to the matrix element given by the expression (27). As follows from this expression not only the  $(j) = (0)$  term, but also the terms with  $(j) \neq (0)$  contribute to the amplitude of this reaction. This fact was known in the theory of cluster knock out reactions for the special case of oscillator shell model wave functions. These  $(j) \neq (0)$  terms correspond to cluster deexcitations according to Ref. [30]. Expression (27) demonstrates that the cluster deexcitation terms appear in the amplitudes of the cluster knock out reactions and similar processes in the general case as well. Despite the fact that in the case of cluster knock out one deals with the final state wave function which was named as an asymptotic one (because in the corresponding wave function components with the eigenvalues  $\varepsilon_\nu \simeq 1$  dominate in the expansion (21)) the sum over  $(j)$  in (27) is not reduced to the trivial term with  $(j) = (0)$ . To demonstrate this let us compare two expressions. In the first one the antisymmetrizer is removed from the right hand side of eq.(22), in the second one — from the left hand side. It is easy to show that they will be equal to each other if the following relation holds

$$Q_{\nu_1} = Q_{\nu_2} (\varepsilon_{\nu_1} = \varepsilon_{\nu_2}) \quad (30)$$

for all terms with  $b_\nu \neq 0$ . However, this is not the case due to the contribution from the terms with  $\varepsilon_\nu \neq 1$ . So, the transition amplitudes from the bound cluster state, even to the asymptotic one, contain the deexcitation terms. In most calculations these terms were not taken into account at all. Some examples of the importance of taking into account this type of exchange terms are given in Refs. [30,31].

Finally, as follows from our analysis, all operators can be subdivided into three groups according to the magnitude of the exchange effects in their matrix elements:

1. Full tensor operators. Their matrix elements are affected maximally when going from the MDM to the AMDM<sub>K</sub>.
2. Pure spatial operators. Their matrix elements are less sensitive to the exchange effects as compared to the first case. If the Pauli forbidden components in the MDM function are eliminated in a thorough way then the exchange effects usually become rather small.

3. Operators whose matrix elements strictly conserved when going from the MDM to the AMDM<sub>K</sub>. They are either pure spin-isospin operators or pure spatial operators being some functions of Casimir operators of SU(3) group.

In most cases the nuclear observables are associated not with a single tensor operator but with their sum. For example, an operator of the magnetic moment has two terms. One comes from the magnetization current and the other from the convective one. If the total angular momentum of the system equals to zero then the contribution of the last term vanishes. More generally, if the spin and isospin of the system under discussion are equal to zero both in the initial and in the final states, then any operator of physical observable appears as an effective spatial operator. In such a case the nucleon exchange effects should not be too large. On the other hand operators of some nuclear observables (for example the operator of M1 transition) at low momentum transfer can be considered with a good approximation as an effective spin-isospin one. In this limit the exchange effects for such matrix elements should be very small.

By this discussion we finish the group-theoretical analysis of nuclear matrix elements. In the next section we will discuss the results of the numerical calculations of the various observables of six-nucleonic systems treating them as  $\alpha$ -2N systems.

### III. SIX-NUCLEON SYSTEM WITHIN THE FRAMEWORK OF THE AMDM

In this section we discuss the AMDM application to the six-nucleon systems (<sup>6</sup>Li and <sup>6</sup>He) treating them as the  $\alpha$ -cluster in its ground state with  $L = S = T = 0$  and two outer nucleons. The Jacoby coordinates for this system together with the conjugated angular momenta are shown in Fig.1.

As an input to the AMDM calculations, the three-body MDM functions  $\Psi(\vec{\rho}, \vec{r})$  named as FUNCTION-92 in Ref. [19] are used. These wave functions were calculated with a large variational basis which includes all important (i.e. with the weight  $P \geq 0.1\%$ ) components with the partial angular momenta  $l, \lambda \leq 4$ .

As has been stated in the Introduction, not the intrinsic cluster wave functions but the corresponding experimental data for the studied observables are used in the calculations within



the MDM. However, when going from the MDM to the totally antisymmetric wave functions one has to use explicitly the intrinsic wave functions of clusters in analogy with the MCM.

The major part of the calculations within the MCM was performed using the simple  $0S^4$  harmonic oscillator shell model function for the  $\alpha$ -particle. Of all possible nucleon correlations only the breathing mode of the  $\alpha$ -particle or the  ${}^3\text{H-p}$  ( ${}^3\text{He-n}$ ) channel was incorporated into the most advanced calculations (see, for example, Ref. [11,13,33]). For many static observables, such a simplified version of the  $\alpha$ -particle wave function does not affect the final result. However, when large momentum is transferred to a multicluster system, then the short-range correlations inside the  $\alpha$ -particle become very important.

Unfortunately, it is known that the  $\alpha$ -particle wave function calculated within a realistic dynamic approach does not reproduce its Coulomb form factor at intermediate momentum transfer, when evaluated in the impulse approximation. To reproduce the experimental data either a very large contribution of the isoscalar exchange current has to be assumed or the existing wave function should be modified to reflect the more complicated dynamic of this system. It seems that such a large contribution of the MEC in the  $\alpha$ -particle, and therefore in the core of the six-nucleon system, is physically not adequate. This is the reason why we decided to modify the  $\alpha$ -particle wave function and did it in a purely phenomenological way. When constructing this wave function we kept in mind that it should have the form convenient for performing the calculation of matrix elements in six-nucleon system with the antisymmetrized wave function of eq. (12).

Following these requirements a phenomenological  $\alpha$ -particle wave function was constructed in Ref. [22]:

$$\Psi = \exp\left(-\frac{\alpha_1}{2} \sum_{k=1}^4 (\vec{r}_k - \vec{R})^2\right) + C \sum_{i=1}^N \exp\left(-\frac{\alpha_1}{2} \sum_{k \neq i} (\vec{r}_k - \vec{R})^2 - \frac{\alpha_2}{2} (\vec{r}_i - \vec{R})^2\right), \quad (31)$$

with the parameters  $\alpha_1 = 0.6144 fm^{-2}$ ,  $\alpha_2 = 6.967 fm^{-2}$  and  $C = -0.4506$ . Within the impulse approximation, this function fits the  $\alpha$ -particle charge form factor in a wide region of momentum transfer. This function was used in Ref. [22] to calculate the  ${}^6\text{Li}$  form factors within the AMDM. A significant improvement of the theoretical description of  ${}^6\text{Li}$  form factors at medium and high momentum transfer was achieved by using this modified  $\alpha$ -particle wave function.

The other advantage of the function (31) consists in its similarity to the oscillator  $OS^4$  one. Their overlap ( $\langle \Psi | \Psi_{osc} \rangle$ ) is larger than 0.9. Therefore one would expect that the qualitative results of the group-theoretical analysis discussed above will be valid in this case as well.

So the model with antisymmetrization is completely defined and we are ready to start presenting the results of calculations within the model. We will discuss below the following three versions of the model:

- the MDM,
- the  $AMDM_C$ , where the normalization with a constant is adopted, and
- the  $AMDM_K$ , where the integral kernel  $\hat{K}$  is used for the renormalization.

#### A. Operators and matrix elements involved in calculation of the observables of the six-nucleon systems.

Three types of tensor operators are involved in our calculations of the various observables of the six-nucleon system. They are:

$$O_{kw}^{um_u, tt_z}(\hat{r}_j) = \tau_{tt_z} f(qr_j) \sum \langle km_k w m_w : um_u \rangle \sigma_{km_k}(j) Y_{wm_w}(\hat{r}_j), \quad (32)$$

$$O_{0w}^{um_u, tt_z}(p_j) = i\tau_{tt_z} f(qr_j) \sum \langle 1m w m_w : um_u \rangle Y_{wm_w}(\hat{r}_j) p_{1m}(j) \quad (33)$$

and

$$O^{um_u, tt_z}(\vec{\sigma}_j \vec{p}_j) = iO_{0u}^{um_u, tt_z}(\hat{r}_j)(\vec{\sigma}_j \vec{p}_j). \quad (34)$$

Here  $\vec{p}$  is the nucleon momentum inside the nucleus and  $q$  is the momentum transfer to the nucleus;  $\tau_0$  and  $\sigma_0$  denote the unit operator ( $k = 0, t = 0$ ) in the isospin and spin space, respectively, and  $\tau_{1z}$  and  $\sigma_{1z}$  are the ordinary isospin and spin operators ( $k = 1, t = 1$ ), respectively;  $f(qr_j)$  is the observable scalar function associated with the process which is being considered.

We designate the nuclear reduced matrix elements associated with the above given operators in the following way:

$$\langle J_f T_f \| O_{kw}^{um_u, tt_z}(\hat{r}_j) \| J_i T_i \rangle = [k w u]_{\Delta T} , \quad (35)$$

$$\langle J_f T_f \| O_{0w}^{um_u, tt_z}(p_j) \| J_i T_i \rangle = [1 w u; p]_{\Delta T} \quad (36)$$

and

$$\langle J_f T_f \| O^{um_u, tt_z}(\vec{\sigma}_j \vec{p}_j) \| J_i T_i \rangle = [0 w u; p]_{\Delta T} . \quad (37)$$

They are specified according to the tensor structure of the corresponding operators. To distinguish the nucleon momentum independent matrix elements (32) from the momentum dependent ones, (33) and (34), the latter will be labeled by an extra index p.  $\Delta T$  reflects the isospin selection rule in the nuclear transitions. If the isospin of both the initial and final states equals to zero then  $\Delta T = 0$ , and if the isospin of one state is T=0 and of the other is T=1 then  $\Delta T = 1$ . Only when both isospins are equal to 1 we have both values;  $\Delta T = 0$  and 1.

In this paper we will discuss:

- the  ${}^6\text{Li}$  and  ${}^6\text{He}$  observables in their ground state,
- the transition  $J^\pi T = 1^+0 \rightarrow 0^+1$  and vice versa generated by various projectiles,
- the  $\gamma$ -transition to the  $J^\pi T = 2^+1$  level and
- the transition  $J^\pi T = 1^+0 \rightarrow J^\pi T = 3^+0$  .

Matrix elements involved in the calculations of the corresponding observables are the following:

1. The ground state of  ${}^6\text{Li}$  ( $\Delta T = 0$ ):
  - i) charge and body (matter) rms radii –  $[000]_0$ ;
  - ii) quadrupole moment –  $[022]_0$ ;
  - iii) longitudinal form factor –  $[000]_0$  and  $[022]_0$ ;
  - iv) magnetic moment –  $[101]_0$  and  $[111; p]_0$ ;

- v) magnetic elastic form factor –  $[101]_0$ ,  $[121]_0$  and  $[111;p]_0$ ;
  - vi) the elastic pion scattering –  $[000]_0$ ,  $[022]_0$ ,  $[101]_0$  and  $[121]_0$ .
2. The ground state of  ${}^6\text{He}$  ( $\Delta T = 0$  and 1):
- i) rms charge radius –  $[000]_0$  and  $[000]_1$ ;
  - ii) rms body radius –  $[000]_0$ .
3. The transition from the ground state of  ${}^6\text{Li}$  to the  $J^\pi T = 0^+1$  level in  ${}^6\text{Li}$  or in  ${}^6\text{He}$  and vice versa:
- i) beta decay –  $[101]_1$ ;
  - ii) muon capture –  $[101]_1$ ,  $[121]_1$ ,  $[011;p]_1$  and  $[111;p]_1$ ;
  - iii) form factor –  $[101]_1$ ,  $[121]_1$  and  $[011;p]_1$ ;
  - iv) positive pion photoproduction –  $[101]_1$  and  $[121]_1$ .
4. The gamma transition to the  $J^\pi T = 2^+1$  level of  ${}^6\text{Li}$ :
- i)  $[101]_1$  and  $[111;p]_1$ .
5. The transition from the ground state of  ${}^6\text{Li}$  to the  $J^\pi T = 3^+0$  level in  ${}^6\text{Li}$ :
- i) gamma transition and electron scattering –  $[022]_0$ ,  $[044]_0$  and  $[112;p]_0$ ;
  - iii) pion scattering –  $[022]_0$ ,  $[044]_0$ ,  $[12u]_0$  and  $[14u]_0$ .

Among the above listed matrix elements only  $[000]_0$ ,  $[022]_0$ ,  $[044]_0$  and  $[1wu;p]_0$  are of pure spatial type. For overlapping clusters, as has been shown in Ref. [22], ordinarily the magnitude of the exchange effects for a pure spatial operator is associated with the quantity  $\delta = 1 - Q^2$ , where  $Q^2$  is given by eq. (29). The MDM functions [19], which are used throughout this paper, were constructed in a way to minimize the admixture of components with Pauli-forbidden Young-schemes  $[f] = [51]$  and  $[6]$  (see Ref. [22]). For this reason the values of  $Q^2$  are rather close to 1 and therefore the exchange effects are usually not large. That is why such observables as  ${}^6\text{Li}$

charge and body radius, quadrupole moment and  ${}^6\text{He}$  body radius should have very close values in all versions of the model. The direct calculations have demonstrated (see Table 1) that the renormalization effects in this group of matrix elements is indeed small.

Matrix elements  $[101]_0$  and  $[101]_1$ , in the long-wave approximation where  $f(qr_j) = \text{Const}$ , are of pure spin and spin-isospin types, respectively. The kernel renormalization restores exactly their values, altered by the C-renormalization. At larger momentum transfer, as follows from Table 1, they depend on the renormalization procedure. Now, let us turn to the discussion of the renormalization effects on various observables of the six-nucleon nuclei.

## **B. The static properties of the six-nucleon systems**

In Table 2 the results of calculation of the static properties of the  ${}^6\text{Li}$  (columns 2–4) and  ${}^6\text{He}$  (columns 5 and 6) are presented.

### *1. Ground state of ${}^6\text{Li}$*

Only one matrix element contributes to the rms radius and the quadrupole moment of  ${}^6\text{Li}$ . Sensitivity of these observables to the version of the renormalization procedure have been discussed above. Here one can only add that the calculated rms radius is in agreement with the experimental data whereas the quadrupole moment is far from the measured one. The theoretical prediction for the value of the quadrupole moment is a special problem and it is beyond the scope of this paper. It seems that one should take into account the D-component of the  $\alpha$ -particle wave function to come close to the experimental value of quadrupole moment of  ${}^6\text{Li}$ . It is worth mentioning that in all large-scale calculations of this moment (see, for example, the discussion in Ref. [22] and references therein) its predicted value is very close to that obtained in this paper.

One can see from Table 2 that both the exchange and renormalization effects for all static observables of six-nucleon system are not large.

## 2. Gamma transition to the $J^\pi T = 2^+1$ level in ${}^6\text{Li}$

The exchange effects in the static characteristics can increase if the leading matrix element of the corresponding operator is suppressed due to nuclear structure effects. Such a situation occurs in  ${}^6\text{Li}$  for the M1  $\gamma$ -transition from the ground state to the  $J^\pi T = 2^+1$  level. Here the magnetization current matrix element  $[101]_1$  is strongly suppressed due to the structure of the corresponding wave functions (the corresponding operator  $O$  is unable to change the total angular momentum  $L$  by two units) and the main contribution comes from the convective current,  $[111; p]$ . So, this transition belongs to the scissor mode. The prediction of the MDM and of two versions of the AMDM differ noticeably from each other:

$\Gamma_{\gamma_0}$  (eV) = 0.29 (MDM), 0.38 (AMDM<sub>C</sub>) and 0.34 (AMDM<sub>K</sub>). The experimental value is  $(0.27 \pm 0.05)$  eV.

The result obtained within the framework of the MDM is closer to that of the AMDM<sub>K</sub>, than to the AMDM<sub>C</sub> one. The AMDM<sub>K</sub> result deviates a little from the measured value. But it is expected that in this hindered transition, the mesonic exchange currents could play a very important role. So it will be interesting to continue to investigate this problem further. Notice that for many other observables the AMDM<sub>K</sub> results are also close to those of the MDM. That is why in these cases the MDM has been very successful in describing these observables.

## 3. Ground state of ${}^6\text{He}$

The neutron halo nucleus  ${}^6\text{He}$  is one of the interesting peculiarities of the six nucleon system. The outer neutron pair, forming this halo, extends to large distances and is localized in the so called quasiasymptotical region. The charge distribution in  ${}^6\text{He}$  is associated with two types of matrix elements –  $[000]_0$  and  $[000]_1$ , contrary to the matter distribution which is associated only with the isoscalar part. So, we can compare the results obtained for two similar operators in the coordinate space which, however, have different isospin structure. This comparison is done in Table 2.

When the kernel renormalization is adopted within the AMDM, the rms radius of  ${}^6\text{He}$  is changed by less than 1% when compared with the MDM case. Let's define, following Ref. [33],

the size of the halo in  ${}^6\text{He}$  as the difference between the proton and neutron radii  $r_{halo} = \langle r_n^2 \rangle^{1/2} - \langle r_p^2 \rangle^{1/2}$ . It changes by about 7% when one goes from the MDM to the AMDM<sub>K</sub> despite its quasiasymptotic nature. The exchange and renormalization effects for the halo in  ${}^6\text{He}$  are not well pronounced. As a rule one should keep in mind this effect when calculating the radius of the halo in heavier nuclei, where the antisymmetrization between nucleons located in different clusters is neglected. More complicated intrinsic structure of the constituent cluster in such systems,  ${}^9\text{Li}$  cluster in  ${}^{11}\text{Li}$  as an example, would increase the exchange effects and, as a result, would increase the calculated halo radius.

The antisymmetrization procedure with renormalization to a constant distorts the asymptotic behavior of the wave function. As a result a nonphysical exchange effect at large distances arises in this case. This is the reason why the body rms radius of  ${}^6\text{He}$  changes when going from the MDM to the AMDM<sub>C</sub>. To avoid this unphysical effect one should deal with the kernel renormalization from the beginning.

#### 4. Beta decay of ${}^6\text{He}$ to ${}^6\text{Li}$

The  ${}^6\text{He}$   $\beta$ -decay rate is determined by the spin-isospin Gamow-Teller operator  $\hat{\sigma}\hat{\tau}$ :

$$ft = \frac{2ft_{0^+ \rightarrow 0^+}}{(g_A/g_V)^2 |M|^2}. \quad (38)$$

We use the following values [34] for the constants in eq. (38):  $2ft_{0^+ \rightarrow 0^+} = 6144 \text{ s}$  and  $(g_A/g_V) = -1.259$ . The results of the  $ft$  calculation are the following:  $ft = 796 \text{ s}$  (MDM and AMDM<sub>K</sub>) and  $772 \text{ s}$  (AMDM<sub>C</sub>). The experimental value of  $ft$  is  $813 \text{ s}$ . Keeping in mind that there should be some meson exchange current contribution, it seems that the calculated value of the  $\beta$ -decay matrix element is somewhat overestimated. The AMDM<sub>K</sub> result is exactly equals to the MDM one, as it should be.

### C. Electromagnetic form factors

### 1. Longitudinal form factors

The results of the calculations of the longitudinal elastic form factor of  ${}^6\text{Li}$  are given in Fig.2. Starting from this figure and in all subsequent ones we present the results in the following way. By the solid line we show the results obtained within the framework of the AMDM<sub>K</sub>, by the dashed line — within the AMDM<sub>C</sub> and by the dotted line — within the MDM. The full elastic form factor consists of the sum of the contributions of the C0 and C2 terms. However the C2 form factor is visible only in the region of the C0 minima which is located at about  $3\text{ fm}^{-1}$ . That is why we are not showing them separately. All longitudinal form factors for transitions between nuclear levels with isospin  $T = 0$  are associated with pure spatial operators. At low momentum transfer the elastic charge form factor of  ${}^6\text{Li}$  is determined by its rms charge radius which is practically not affected by the nucleon exchange. More importantly, the exchange effects remain very small up to a high momentum transfer. The effects of the kernel renormalization are too small to be seen in the Fig.2. So, one can safely use the MDM for this elastic longitudinal form factor calculations.

As it had been discussed earlier in Ref. [22] and confirmed by the present calculation, in order to reproduce the  ${}^6\text{Li}$  elastic form factor it is very important to use the correlated  $\alpha$ -cluster wave function which reproduces the  $\alpha$  form factor. Otherwise, the calculated high momentum part of the  ${}^6\text{Li}$  elastic form factor will be much lower than the measured one.

The antisymmetrization results in the mixing of the components of the three-body functions which have different partial angular momenta  $l$  and  $\lambda$  but the same total  $L$ . In the  ${}^6\text{Li}$  ground state wave function this situation is not well pronounced, because the dominant weight is associated with the  $l = \lambda = L = 0$  component. In the wave function of the  $J^\pi T = 3^+0$  level in  ${}^6\text{Li}$  there are already two such components:  $l = 2, \lambda = 0$  and  $l = 0, \lambda = 2$  with the total angular momentum  $L = 2$  and spin  $S = 1$ . The antisymmetrization with renormalization results in their additional mixing, which differs essentially from the MDM mixing. For the same reason there is noticeable difference in the wave functions of this level in the two versions of the AMDM - with and without kernel renormalization. Thus the modification of this inelastic longitudinal form factor due to the antisymmetrization and renormalization should be rather large.



Fig.3 displays the  $\sqrt{B(q^2, E2)}$ —the square root of the reduced quadrupole transition strength to this level at low momentum transfer region. Just this multipole dominates in the form factor for this transition. The kernel renormalization effects are visible already at zero momentum transfer due to this additional mixing. At photon point  $B(E2, 1^+0 \rightarrow 3^+0)$  in  $e^2fm^4$  equals to 20.05, 15.25 and 20.71 for the MDM, AMDM<sub>C</sub> and AMDM<sub>K</sub> models, respectively. The experimental value is  $21.8 \pm 4.8$  [39]. So, more precise measurement of this observable seems to be needed to test the theoretical models. Fig.4 displays the form factor for this transition in a broad region of momentum transfer. In logarithmic scale, it is not easy to see the difference between the three versions of the model. In the region of the first maximum this difference is about the same as in the region of very low momentum transfer. The magnitude of the calculated form factor is lower than the experimental one. The reason for this is not clear enough. At high momentum transfer, for example, it is possible that noncentral components of the  $\alpha$ -particle wave function, which are not taken into account at all, start to play a role. So, this discrepancy should be a subject of further studies.

## *2. Magnetic form factors*

The earlier MDM calculations of the  ${}^6\text{Li}$  magnetic form factors in Ref. [40] have demonstrated quite clearly that despite of a good agreement with experimental data in the region of the first maximum, the theoretical result for the region of the second maximum lies much below the experimental data for any choice of NN and  $\alpha$ -N interaction [40,41]. At the same time, the studies carried out in Ref. [22] showed qualitatively that the antisymmetrization is of great importance when one calculates the  ${}^6\text{Li}$  transversal form factors. Both the elastic and the inelastic transversal form factors to the  $J^\pi T = 0^+1$  level are governed by the M1 multipole only. The antisymmetrization of the wave function leads to a strong increase of the form factor within the region of the second maximum, thereby improving the agreement with the experimental data substantially. This is demonstrated in Fig.5 and Fig.6.

At low momentum transfer the M1 operator is proportional either to the operator of the magnetic moment (in the case of the elastic scattering) or to the GT-operator of  $\beta$ -decay and has

mainly a spin-isospin component. Here we use the fact that the convective current contribution is small. That is why the exchange effects are very small in this region of momentum transfer. However, already at the second maximum their role becomes crucial because the spatial part of the M1 operator starts to play its decisive role.

It is necessary to stress that in the AMDM<sub>K</sub> version the position of the minimum is reproduced very precisely. The other interesting effect of kernel renormalization consists in stabilization of the AMDM results for intermediate momentum transfer ( $q \leq 2.5 - 3.0 fm^{-1}$ ): the magnitude of the form factors in the region of the second maximum becomes almost independent on the details of the  $\alpha$ -cluster wave function. It means that in this region the exchange and short-range correlation effects are well separated from each other. This result is very important because our  $\alpha$ -cluster wave function has a pure phenomenological origin.

At larger momentum transfer an interference between two types of nucleon correlations (exchange and short-range) starts to play its decisive role. The consistent treatment of both effects results in appearance of a third maximum in the M1 form factors at about  $q^2 \simeq 20 fm^{-2}$ . Again as it happened with the second maximum, the AMDM<sub>K</sub> version provides more stability of the third maximum in the magnetic form factor as compared to the AMDM<sub>C</sub> version.

Elastic M1 form factor has an isoscalar nature. Therefore, the exchange currents in this case are not very strong and should not alter considerably the results for small and moderate momentum transfer (see discussion in Ref. [22]). The inelastic M1 form factor has an isovector origin and it is somewhat lower than the experimental data, already at lower momentum transfer. One can assume that this is a real indication for the mesonic exchange currents in this transition. At higher momentum transfer their contribution should increase.

It seems to us that it is very promising to continue the experimental study of  ${}^6\text{Li}$  form factors and to cover the high momentum transfer region. This can be an interesting topic, for example, in CEBAF.

### D. Gamow-Teller transition in muon capture

The Gamow-Teller transitions in muon capture on nuclei are interesting from the following points of view:

- how well the nuclear models are able to predict their strength at intermediate momentum transfer,

- what is the magnitude of the induced pseudoscalar coupling  $g_P$  in nuclei,

- how large are the mesonic exchange currents at this momentum transfer.

Up to now these problems have been analyzed in great details only in the few-body systems.  ${}^6\text{Li}$  gives the other opportunity to study the above discussed problems in a nucleus with twice as many nucleons as  ${}^3\text{He}$ . Here, all these effects can be enhanced.

The momentum transfer in muon capture on  ${}^6\text{Li}$  with formation of  ${}^6\text{He}$  in its ground state is equal to  $|\vec{q}| = E_\nu/c = 100.7 \text{ MeV}/c$ . This value is in the region of the first maximum in the inelastic electron scattering form factor (see Fig.6) to the  $J^\pi T = 0^+ 1$  level of  ${}^6\text{Li}$ . Four matrix elements form two transition amplitudes,  $T_1$  and  $T_2$ , to the ground state of  ${}^6\text{He}$ :

$$T_1 = \frac{2G_A[101]}{3}\{1 - \Delta T_1\} \quad (39)$$

and

$$T_2 = (2/9)^{1/2}(G_A - G_P)[101]\{1 + \Delta T_2\}. \quad (40)$$

Here we have isolated the dominant matrix element [101] from the rest.  $\Delta T_1$  and  $\Delta T_2$  are built up from the three others, [121], [111p] and [011p]:

$$\Delta T_1 = \sqrt{1/2}\frac{[121]}{[101]} + \sqrt{3/2}(g_V/G_A)\frac{[111p]}{M_N[101]} \quad (41)$$

and

$$\Delta T_2 = \sqrt{2}\frac{[121]}{[101]} + \frac{3g_A}{G_A - G_P}\frac{[011p]}{M_N[101]}. \quad (42)$$

$G_A$  and  $G_P$  are some combinations of the weak interaction coupling constants. They are given in Appendix A together with the expression for the capture rate.

Two observables are of experimental interest in this partial muon capture transition – the capture rate  $\Lambda$ , when the hyperfine states are populated according to their statistical weights, and the ratio of the capture rates from the upper,  $\Lambda_+$ , and the lower,  $\Lambda_-$ , hyperfine states of the  ${}^6\text{Li}$  mesic atom.

The capture rate is proportional to the sum of  $T_1^2$  and  $T_2^2$ , the ratio  $\Lambda_+/\Lambda_-$  is given by the following expression:

$$\Lambda_+/\Lambda_- = \frac{G_P^2}{\{3G_A - G_P\}^2} \{1 + \Delta_2\}, \quad (43)$$

where

$$\Delta_2 = \frac{3(G_P - G_A)}{2G_P} \left\{ 1 - \frac{3}{2X} \left[ 1 - \frac{G_P}{3G_A} \right] \right\}^{-1} \quad (44)$$

and

$$X = \frac{\Delta T_1 + \Delta T_2}{1 + \Delta T_2}. \quad (45)$$

It is through  $X$  that the nuclear structure is manifested in the ratio of the capture rates  $\Lambda_+/\Lambda_-$ . In the limit  $\Delta T_1$  and  $\Delta T_2 \rightarrow 0$ ,  $X$  and  $\Delta_2$  are equal to zero and this ratio is given by the coupling constants only showing a strong dependence on  $g_P$ . That is why this ratio is a subject of detailed analysis in many nuclei (see Ref. [43]).

$\Delta T_1$  is independent of  $g_P$ . After fixing the weak interaction constants according to Appendix A one arrives to the values of  $T_1$  and  $\Delta T_1$  listed in Table 3. As follows from Table 3, the combination of matrix elements which forms  $\Delta T_1$  is sensitive to the nuclear model. But again, the result in the AMDM<sub>K</sub> version is closer to the MDM one. The difference is about 10%. The full amplitude  $T_1$  is less sensitive to the model because  $\Delta T_1$  itself is about half of a per cent. The combination of the matrix elements which forms  $\Delta T_2$  is not very sensitive to the model as well. But its relative weight in the full amplitude  $T_2$  is about 15 %.

In both cases it is important to take into account the velocity dependent matrix elements (the corresponding operator is proportional to the momentum of nucleon inside the nucleus) . If one neglects them (see last column of Table 3), as it is done in some papers, then both terms,  $\Delta T_1$  and  $\Delta T_2$ , will be changed drastically.

The ratio of the hyperfine capture rates depends on the nuclear model through  $X$  sensitivity of the amplitudes and their combinations to the nuclear model we give in Table 3 their magnitudes for fixed value of the induced pseudoscalar coupling constant ( $g_P/g_A = 7$ ). Finally, for the same value of the coupling constant we give the capture rate and the ratio  $\Lambda_+/\Lambda_-$ .

Fig.7 demonstrates the calculated capture rate as a function of  $g_P/g_A$  together with experimental data [44]. They are far from each other. Even if one increases arbitrarily the theoretical capture rate by about 10% , to take into account in this way the meson exchange current contribution, the situation improves only slightly. But nevertheless, the value of the induced pseudoscalar constant which is needed to reproduce the experimental data is lower than that which follows from the Goldberger-Treiman relation. It seems very desirable to remeasure this capture rate with a better accuracy to insure that situation is not due to the existing experimental data.

Fig.8 demonstrates the predicted values for the ratio of the capture rates as a function of  $g_P/g_A$  for the three versions of the model. The absolute value of this ratio appears to be the same within about 3%. It means that the uncertainty from the nuclear structure side is minor. As the next step, one should incorporate into the calculations the meson exchange currents, which can modify the result obtained for the ratio of the capture rates.

### **E. Partial transitions in pion scattering and pion photoproduction off ${}^6\text{Li}$**

After successfully employing the developed model for description of the  ${}^6\text{Li}$  traditional observables let us turn our attention to the:

- pion elastic and inelastic scattering with the excitation of the  $J^\pi T = 3^+0$  level,
- pion photoproduction with the formation of  ${}^6\text{He}$  in its ground state ( $J^\pi T = 0^+1$ ).

These reactions are selected for the following reasons. Pion scattering on polarized target has already been carried out and the vector analyzing power  $iT_{11}$  for the ground state and the  $J^\pi T = 3^+0$  level transitions was measured. Nuclear models can be tested in a more thorough way via the polarization observables than via the differential cross sections, provided that the reaction mechanisms are properly taken into account. So, pion scattering can be considered as

complementary to electron scattering in probing details of the  ${}^6\text{Li}$  structure. One can invert the formulation of the problem — if the nuclear structure is well determined, then the other ingredients of the theory can be checked.

As to the pion partial photoproduction off nuclei it is expected that very soon the data with polarized photons will be available as well. It will be data on the beam asymmetry:

$$\Sigma(\theta) = \frac{\sigma^\perp(\theta) - \sigma^\parallel(\theta)}{\sigma^\perp(\theta) + \sigma^\parallel(\theta)}, \quad (46)$$

where  $\theta$  is the polar angle of the outgoing pion,  $\sigma^\parallel$  is the differential cross section for the photon polarization along the  $x$  axes, and  $\sigma^\perp$  — along the  $y$  axes. The pion momentum  $\vec{q}$  is directed along the  $x$  axes, the photon momentum  $\vec{k}$  along the  $z$  axes and the vector  $[\vec{k} \times \vec{q}]$  along the  $y$  axes. We will demonstrate that, depending on the momentum transfer (pion emission angle), there are regions sensitive either to the nuclear model or to the details of the reaction mechanism. At present there are polarization measurements in pion photoproduction when nucleon knocked out from nucleus. Pion scattering and pion photoproduction on light nuclei were described very successfully within the framework of DWIA in momentum space (see for example Ref. [45,46]). However, in some cases (including elastic and inelastic to the  $3^+0$  level scattering in  ${}^6\text{Li}$ ) one has to use the coupled channel method (see for example Ref. [47]).

In this paper we will continue to exploit the coupled channel method for pion scattering to the ground state, the  $J^\pi T = 1^+0$  and the  $3^+0$  levels, in line with Ref. [47]. Pion photoproduction will be analyzed within the framework of the DWIA, in line with Ref. [46]. Some basic formulas for both processes are given in Appendix B.

Among all low lying states of  ${}^6\text{Li}$  the elastic and the inelastic to the  $3^+0$  cross sections are measured for several energies. Cross sections to these levels are large due to the isoscalar nature of the nuclear transitions. More or less complete data, which include the polarization observables, exist for a few energies of the incoming pions. One of such energy is  $T_\pi = 134$  MeV. That is why we will concentrate all our attention mainly on the data at this energy.

1. *Elastic and inelastic to the  $J^\pi = 3^+0$  level pion scattering*

Elastic and inelastic to the  $3^+0$  level pion scattering off  ${}^6\text{Li}$  are governed by the spin independent part of the elementary  $\pi\text{N}$  scattering amplitude. The spin-dependent part of pion-nucleon amplitude is much smaller and does not show up in the differential cross section. In this section we compare our results with the experimental data of Ref. [47].

Fig.9 displays the elastic cross section for 134 MeV pions. All three versions of the model give similar results. The situation is the same as in the case of electron scattering where the calculated longitudinal form factors appeared very close to each other. The point is that in pion scattering at this energy the maximal momentum transfer does not exceed  $2.5\text{ fm}^{-1}$  where these three versions of the model predict very close values for the matrix element — see Table 1.

In the case of the  $3^+0$  level the  $\text{AMDM}_\text{C}$  version at low momentum transfer region (small angles) gives the lowest result just as in the electron scattering case (see Fig.10). The  $\text{MDM}$  and  $\text{AMDM}_\text{K}$  versions predict a higher value which is more close to the experimental data. Predictions of all three versions of the model in the region of the minimum differ from each other significantly.

In both cases one can say that agreement between theory and experiment is quite good and some deviation of the theory from experiment can be due to some shortcomings associated with the reaction part. For example in this calculation the pion absorption is ignored. Of course this process can not play a decisive role, but it can have some effects.

Contrary to the differential cross section the vector polarization  $T_{11}$  is caused by interference between the spin-dependent and the spin-independent parts of the pion-nucleon amplitude. To have some feeling of  $T_{11}$  it is instructive to use the plane wave approximation, following Ref. [48]. In the elastic longitudinal electron scattering form factor one could safely neglect the  $L=2$  matrix elements. The same is true for the pion scattering. Then in the plane wave approximation one gets

$$iT_{11}(d\sigma/d\Omega) \sim [000][101]Im[f_{\pi N}(s=0)f_{\pi N}^*(s=1)]. \quad (47)$$

Here  $f_{\pi N}(s=0)$  and  $f_{\pi N}(s=1)$  are the spin-independent and spin-dependent parts of the elementary  $\pi\text{N}$  scattering amplitudes, respectively. From this expression it follows that  $iT_{11}$

changes its sign where the M1 form factor does. The largest value of the vector analyzing power corresponds to the minimum in the differential cross section of pion scattering. The  $Im[f_{\pi N}(s=0)f_{\pi N}^*(s=1)]$  changes its sign at  $\theta$  larger than  $120^\circ$  for  $T_\pi > 120$  MeV. Thus the vector analyzing power is a complicated function of the scattering angle.

The vector analyzing power  $iT_{11}$  for the transition to the  $3^+0$  level in the plane wave approximation looks very similar:

$$iT_{11}(d\sigma/d\Omega) \sim [022]\{[122] + (32/49)^{1/2}[123]\}Im[f_{\pi N}(s=0)f_{\pi N}^*(s=1)]. \quad (48)$$

The results of comparison between experimental data and the three versions of the model is given in Fig.11 for the elastic scattering and in Fig.12 for the transition to  $J^\pi T = 3^+0$  level.

Contrary to the differential cross section the vector analyzing power is more sensitive to the nuclear model. All three versions of the model used in the calculations give different results. The AMDM<sub>K</sub> version explains the shape of the vector polarization as a function of scattering angle. There is some discrepancy in the magnitude of the vector analyzing power. This discrepancy can be caused by the approximate treatment of the pion-nuclear dynamic. But what emerges from the calculations is that the nuclear model is already reliable enough so one can begin to improve upon the dynamic. Simultaneously it seems to be very useful to have more precise experimental data on this quantity.

### F. Pion photoproduction to the ${}^6\text{He}$ ground state.

Pion photoproduction at threshold is dominated by the Kroll-Ruderman spin-flip term. So in the pion photoproduction on  ${}^6\text{Li}$  with formation of  ${}^6\text{He}$  in its ground state the same matrix elements governing the transition as in muon capture and in electron scattering. So at threshold one expects a successful description of experimental data. In Fig.13 the calculated results within the framework of the AMDM<sub>K</sub> are compared to experimental data of Ref. [49,50] at 200 MeV energy of the incoming photons. At this energy the momentum transfer is covered from  $0.5 \text{ fm}^{-1}$  at  $25^\circ$  to  $1.5 \text{ fm}^{-1}$  at  $135^\circ$ . At this end point pion photoproduction is governed by the form factor of electron scattering in its minima, where it is very difficult to expect a precise theoretical



description of the momentum dependence. That is why at backward angles there is a serious disagreement between theory and experiment. As to the forward angles one sees a nice agreement with experimental data.

At higher energies of incoming photons, say at 320 MeV, contribution of  $\Delta$ -isobar becomes very important and it brings the spin-independent part into the amplitude. At this energy the difference in the differential cross section between the three versions of the model is very small at forward angles which correspond to low momentum transfer. Fig.14 demonstrates this in a clear way. Predictions become different from each other starting from the angle  $\theta$  at about  $60^\circ$ .

The beam asymmetry at forward angles is also weakly sensitive to the model — see Fig.15. At these angles a strong sensitivity of the beam asymmetry to the  $\Delta$ -isobar property inside a nucleus is found. In Fig.16 the beam asymmetry is plotted as a function of the  $\Delta$ -isobar mass,  $M_\Delta$ , in nuclei. A 5% deviation of this mass from its free value changes the beam asymmetry noticeably. This happens in the region of angles from  $20$  to  $40^\circ$  where the cross section is not small. So, this result can be considered as a motivation for measuring the beam asymmetry in this transition. Variation of the  $\Delta$ -isobar mass affects the differential cross section mainly at backward angles (Fig.17). However at these angles there is a strong sensitivity to the nuclear model as well.

#### IV. CONCLUSION

A modified version of the Multicluster Dynamic Model was proposed to construct completely antisymmetrized wave functions of multicluster systems. In the model the intrinsic wave functions of the constituent clusters were inserted explicitly, and as a result the model became closer to the MCM, where the motion of all nucleons is taken into account on equal ground. However, contrary to the MCM, the cluster-cluster potentials used are those constructed on the basis of phase shifts analysis of the free cluster scattering and thus the on-shell properties of these potentials are taken into account in the most precise way. Such a modification, nevertheless, retains the easy application of the MDM and at the same time allows us to incorporate into the calculations the realistic wave functions which describe the motion of the nucleons inside the clusters.

A group-theoretical analysis of matrix elements for arbitrary multicluster systems was developed. On its basis all operators of single-particle origin have been classified according to their response to the antisymmetrization procedure. A group of operators is found whose matrix elements are strictly conserved when going from the MDM to the AMDM<sub>K</sub>, but not to the AMDM<sub>C</sub>. This analysis allows to predict, before the numerical calculations are carried out, how essential will the exchange effects be for the particular nuclear characteristic. Simultaneously, it was shown that the kernel renormalization removes the spurious effects which had appeared when the renormalization to constant was adopted.

Detailed numerical calculations of various observables in the six nucleon systems were performed. These nuclei are particularly singled out in nuclear physics because they already exhibit quite properly the typical properties of all light nuclei, but at the same time the number of nucleons is not too large to prevent an accurate and consistent calculations starting from the realistic interactions.

Within the framework of the AMDM<sub>K</sub> a better description of many six-nucleon observables has been achieved. The electron scattering form factors are those obtained with high precision. One of the interesting effects of the kernel renormalization consists in the stabilization of the AMDM results for intermediate momentum transfer ( $q \leq 2.5 - 3.0 fm^{-1}$ ): the magnitude of the magnetic form factors in the region of the second maximum became almost independent on the details of the  $\alpha$ -cluster wave function. It means that in this region the exchange and short-range correlation effects are well separated from each other. This result is very important for the accuracy of the model because our  $\alpha$ -cluster wave function has a pure phenomenological origin.

At larger momentum transfer an interference between two types of nucleon correlations (exchange and short-range) starts to play its decisive role. The consistent treatment of both effects results in the appearance of a third maximum in the M1 form factors at  $q^2 \simeq 20 fm^{-2}$ . And again the AMDM<sub>K</sub> version provides some stabilization of this maximum.

The model developed was applied to muon capture, pion scattering and pion photoproduction. It succeeded in providing a good description of the differential cross sections in pion scattering. What is more important, it allowed us to reproduce at least the shape of the vector polarization which is more sensitive to the details of nuclear structure. Thus we have demonstrated that the

AMDM<sub>K</sub> allows us to accurately describe tiny details of the nuclear structure which, nevertheless, are essential for the interpretation of the polarization phenomena in nuclear reactions.

In the case of pion photoproduction, a region of angles was found where the beam asymmetry depends only slightly on the nuclear model and very strongly on the mass of the  $\Delta$ -isobar inside nuclei. Experimental data in this region of angles, if they appear, can provide fresh insight into this problem.

The calculations performed have demonstrated that the results of the group-theoretical analysis are valid in a more realistic case as well, when the cluster wave functions are more complicated as compared to the SU(4) and SU(3) scalars.

There is one more aspect of this paper which can be formulated in the following statement: after introducing the kernel renormalization the model became more universal and can be applied now to more heavy multicluster systems, contrary to the MDM.

The group-theoretical analysis carried out in this paper offers promise as a processing tool and can be used in many other situations. Here we would like to demonstrate two more areas of its application. For a certain (and rather wide) type of light systems the many nucleon wave functions constructed within the framework of the oscillator shell model can be rewritten in bi-[51] or multicluster [52] representation. In other words such a wave function can be represented by eq.(12) where the  $\alpha$ -particle,  $^{16}\text{O}$ , etc., and nucleons act as clusters. So the group theoretical analysis may be applied to such systems as well. From this analysis one is able to get early insight on the role of the nucleon exchange in the discussed systems and to estimate its effect arising from the antisymmetrization between nucleons in different clusters. We will not discuss all these issues because they are beyond the scope of this paper.

There is another interesting field of application for the developed scheme of the group-theoretical analysis. The case in point is the problem known as quarks inside the nuclei. If one starts from the three-quark representation of the individual nucleons in nuclei (and does not take into account contribution of "sea"), then the question whether one should take into account the quark degrees of freedom of nuclei, or it would be enough to consider only the nucleons as constituents of nuclei, depends substantially on the magnitude of the quark exchange effects.

Indeed, as we have seen, in the multicluster system any process without the breaking down

of the constituent clusters can be described within the framework of the approaches where the clusters themselves are treated as an elementary particle. Such an approach is valid when the exchange effects between clusters are small.

To estimate the quark exchange effects in nucleus it is again convenient to use the methods of group-theoretical analysis. Let us discuss very qualitatively two conclusions which follow from such an analysis.

1. The exchange effects should be larger for observables which are described by the full tensor operator. However even in this case the quark exchange effects in nuclei are usually rather small because of high internucleon distances. That is why the quark degrees of freedom are seen in such processes only at very high momentum transfer.

2. Simultaneously from our analysis (by reduction *ab absurdam*) it follows that the quark effects in nuclei should be more pronounced in processes where the break down of the quark clusters or their excitation take place. Such processes are enhanced due to the exchange effects [53]. One interesting example is already considered in Ref. [54], where the nucleon resonance as a spectator participates in the reaction. Though the weight of the components with the nucleon resonance in the nuclear ground state wave function is very small, observation and investigation of the corresponding reaction is important due to more transparent manifestation of the quark degrees of freedom in nuclei in this case.

Thus, we have shown in this paper that the group-theoretical analysis can open a new way for general investigation of exchange effects in various nuclear and subnuclear processes. Some specific examples have been discussed, for example, in Ref. [54].

## ACKNOWLEDGMENTS

This work is supported in part by the National Science Foundation under Grant # PHY-9413872 and Russian Foundation of Basic Research Grants # 96-02-18691.

R.A.Eramzhyan would like to express his thanks to the Cyclotron Institute at Texas A&M University for the kind hospitality.

The authors would like to thank A.A.Chumbalov and S.S.Kamalov for cooperation in the ini-

tial stage of this work concerning the pion physics, S.Shlomo for careful reading our manuscript and many valuable suggestions and V.I.Kukulin and V.N.Tolstoy for the numerous fruitful discussions.

## APPENDIX A: GENERAL EXPRESSIONS FOR MUON CAPTURE RATES

The muon capture rate is expressed via the amplitudes given by eqs.(39) and (42) in the following way:

$$\Lambda = 8\pi^3 \alpha^3 (m_\mu/m_e)^5 \ln 2 \eta(E_\nu) Z^3 R_Z \frac{1}{2ft_{0^+ \rightarrow 0^+}} \frac{(2J_f + 1)}{(2J_i + 1)} \{T_1^2 + T_2^2\}. \quad (\text{A1})$$

Here

$$\eta(E_\nu) = (E_\nu/m_\mu)^2 \left\{ 1 - \frac{E_\nu}{m_\mu + M_i} \right\} \left[ \frac{1}{1 + m_\mu/M_i} \right]^3. \quad (\text{A2})$$

$R_Z = 0.92$  is the dimensionless quantity and is equal to the ratio between the averaged muon wave function squared over the nuclear volume and its value for the point nucleus at the origin,  $Z$  is the charge of  ${}^6\text{Li}$  and  $M_i$  is its mass.  $M_N$  is the nucleon mass.

After eliminating the main matrix element [101] from the amplitudes  $T_1$  and  $T_2$  one comes to the following expression for the sum of  $T_1^2$  and  $T_2^2$ :

$$T_1^2 + T_2^2 = \frac{2G_{G-T}^2 [101]^2}{3} \{1 + \Delta_1\} \quad (\text{A3})$$

where

$$G_{G-T}^2 = G_A^2 + G_P^2/3 - 2G_A G_P/3 \quad (\text{A4})$$

is the square of the Gamow-Teller constant in muon capture,

$$\Delta_1 = \frac{2G_A^2}{3G_{G-T}^2} \{\Delta T_1^2 - 2\Delta T_1\} + \frac{(G_A - G_P)^2}{3G_{G-T}^2} \{\Delta T_2^2 + 2\Delta T_2\} \quad (\text{A5})$$

and

$$G_A(q^2) = g_A(q^2) - 4.706 g_V(q^2) \frac{E_\nu}{2M_N}, \quad (\text{A6})$$

$$G_P(q^2) = \{g_P(q^2) - g_A(q^2) - 4.706g_V(q^2)\} \frac{E\nu}{2M_N}, \quad (\text{A7})$$

where  $g_A$  is the axial-vector coupling constant,

$$g_A(q^2)_\mu/g_V(0) = -1.239, \quad (\text{A8})$$

and

$$g_A(0)/g_V(0) = -1.259. \quad (\text{A9})$$

$g_V$  is the vector coupling constant

$$g_V(q^2)/g_V(0) = 0.972, \quad (\text{A10})$$

and  $g_P$  is the induced pseudoscalar coupling constant, which is less known compared to the two others. It is fixed by the Goldhaber-Treiman relation [55] to be

$$g_P(q^2)/g_A(0) = 6.78. \quad (\text{A11})$$

Ordinary calculation results are given versus this coupling constant.

## APPENDIX B: GENERAL FORMALISM FOR PION SCATTERING AND PION PHOTOPRODUCTION

The starting point for pion scattering and pion photoproduction calculations is the construction of the multiple scattering matrix  $T(E)$ . It is obtained as a solution of the Lippmann-Schwinger equation

$$T(E) = V(E) + V(E)\hat{P}G(E)T(E). \quad (\text{B1})$$

Here  $G(E)$  is the pion-nucleus Green's function,  $V(E)$  is a potential matrix, and  $\hat{P}$  is a projection operator. Projection to the nuclear ground state corresponds to application of the optical model, whereas projection into a group of nuclear states corresponds to the application of the coupled channel method.

The potential matrix is usually divided into a microscopic first order term  $V_1(E)$  and a phenomenological second order term  $V_2(E)$  :  $V(E) = V_1(E) + V_2(E)$ . The potential matrix  $V_1(E)$  contains the full spin and isospin dependence of the pion nucleon amplitudes via the impulse approximation and receives contributions from the nuclear matrix elements. The second order term is associated with true pion absorption and higher order processes. As follows from Ref. [46] this term is weak in  ${}^6\text{Li}$ . To simplify the calculations we neglect this term.

The pion photoproduction off nuclei is treated by the DWIA method. The pion photoproduction matrix is obtained from the equation similar to that in eq.(B1):

$$T_{\pi\gamma} = U_{\pi\gamma} + T'_{\pi\pi'}G(E)U_{\pi\gamma}. \quad (\text{B2})$$

Here  $U_{\pi\gamma}$  is the plane wave photoproduction amplitude off nuclei,

$E(q) = E_\pi(q) + E_A(q)$  is the total energy of the pion-nuclear system. The auxiliary matrix  $T'$  is related to the pion-nuclear scattering T-matrix discussed above by the following way:

$$T'(\hat{q}, \hat{q}_0) = [(A - 1)/A]T(\hat{q}, \hat{q}_0). \quad (\text{B3})$$

In the Impulse Approximation the matrix elements of  $U_{\pi\gamma}$  are expressed in terms of the elementary  $(\gamma, \pi)$  amplitude. In our calculations the Blomqwist-Laget amplitude for pion photoproduction (see Ref. [56]) is used.

## REFERENCES

- <sup>1</sup> B.S.Pudliner, V.R.Pandharipande, J.Carlson and R.B.Wiringa, Phys. Rev. Let. **74**,4396 (1995)
- <sup>2</sup> V.I.Kukulin and V.M.Krasnopol'sky, J.Phys. **G3**, 795 (1977)
- <sup>3</sup> K.Varga and Y.Suzuki, Phys. Rev **C52**, 2885 (1995)
- <sup>4</sup> G.L.Strobel. Phys. Rev. **C18**, 2395 (1978)
- <sup>5</sup> A.M.Gorbatov, Yadernaya Fizika **55**, 1791 (1992)
- <sup>6</sup> D.C.Zheng, B.R.Barrett, J.P.Vary, W.C.Haxton and S.-L.Song, Phys.Rev. **C52**, 2488 (1995)
- <sup>7</sup> R.F.Bishop, M.F.Flynn, M.C.Boscá, E.Buendía and R.Guardiola, Phys. Rev. **C42**, 1341 (1990)
- <sup>8</sup> J.A.Weeler, Phys.Rev. **52**, 1083 (1937)
- <sup>9</sup> K. Langanke, Advances in Nuclear Physics **21**, 85 (1994), Eds. J. W. Negele and E. Vogt, Plenum Press, New York - London
- <sup>10</sup> K.Varga, Y.Suzuki and Y.Ohbayasi, Phys.Rev. **C50**, 189 (1994)
- <sup>11</sup> K.Varga, Y.Suzuki and I.Tanihata, Phys.Rev. **C52**, 3013 (1995)
- <sup>12</sup> K.Wildermuth and Y.Tang, A unified theory of the nucleus. Vieweg/Braunschweig, 1977
- <sup>13</sup> Y.Fujiwara and Y.C.Tang, Few-Body Systems **12**, 21 (1992)
- <sup>14</sup> A.T.Kruppa, R.Beck and F.Dickmann, Phys. Rev. **C36**, 327 (1987)
- <sup>15</sup> T.Kajino, T.Matsue and A.Arima, Nucl.Phys. **A423**, 323 (1984)
- <sup>16</sup> S.Weber, M.Kachelrieß, M.Unkelbach and H.M.Hofmann, Phys.Rev. **C50**, 1492 (1994);  
M.Unkelbach and H.M.Hofmann, Few-Body Systems **11**, 143 (1991)
- <sup>17</sup> M.N.Ustinin and V.D.Efros Yad.Fiz. (Sov.J.Nucl.Phys.) **49**, 1297 (1989)
- <sup>18</sup> V.I.Kukulin, V.G.Neudatchin, Yu.F.Smirnov and I.T.Obukhovskiy, Clusters as Subsystem in Light Nuclei (In the book series: Clustering Phenomena in Nuclei, V.III. Vieweg and Sohn, Braunschweig/Wiesbaden, 1982)



- <sup>19</sup> V.I.Kukulin, V.N.Pomerantsev, Kh.D.Rasikov, V.T.Voronchev and G.G.Ryzhikh, Nucl.Phys. **A586**, 151 (1995)
- <sup>20</sup> V.T.Voronchev, V.I.Kukulin, V.N.Pomerantsev, Kh.D.Rasikov and G.G.Ryzhikh, Yad.Fizika. **57**, 1964 (1994)
- <sup>21</sup> M.V.Zhukov, B.V.Danilin, D.V.Fedorov, J.M.Bang, I.J.Thompson and J.S.Vaagen, Phys.Rep., **231**, 151 (1993)
- <sup>22</sup> G.G.Ryzhikh, R.A.Eramzhyan, V.I.Kukulin and Yu.M.Tchuvil'sky, Nucl.Phys. **A563**, 247 (1993)
- <sup>23</sup> R.A.Eramzhyan, G.G.Ryzhikh, V.I.Kukulin and Yu.M.Tchuvil'sky, Phys.Lett. **B228**, 1 (1989)
- <sup>24</sup> G.G.Ryzhikh, Yu.M.Tchuvil'sky and R.A.Eramzhyan, Frontiers in Nuclear Physics , Dubna D4-95-308, 1995, p.223
- <sup>25</sup> V.I.Kukulin, G.G.Ryzhikh, R.A.Eramzhyan and Yu.M.Tchuvil'sky, Izvestiya Academy Nauk USSR, ser. fiz., **v.57**, 39 (1993)
- <sup>26</sup> V.I.Kukulin, G.G.Ryzhikh, T.Yu.Tretiakova, Yu.M.Tchuvil'sky and R.A.Eramzhyan, Preprints Inst. for Nucl. Res. Acad. of Sci. USSR, P-0650 and P-0651, Moscow (1989); P-0685, Moscow (1990)
- <sup>27</sup> S.Saito, Progr. Theor.Phys (Suppl.) **62**, 11 (1977)
- <sup>28</sup> S.Saito, Progr. Theor. Phys **41**, 705 (1969)
- <sup>29</sup> V.M.Krasnopolsky and V.I.Kukulin, Yad. Fiz. **20**, 883 (1974)
- <sup>30</sup> V.G.Neudatchin, A.A.Sakharuk, W.W.Kurowsky and Yu.M.Tchuvil'sky, Phys.Rev. **C50**, 148 (1994);
- <sup>31</sup> Yu.M.Tchuvil'sky, W.W.Kurowsky, A.A.Sakharuk, and V.G.Neudatchin, Phys.Rev. **C51**, 784 (1995)
- <sup>32</sup> I.Tanihata, D.Hirata, T.Kobayashi, S.Shimoura, K.Sugimoto and H.Toki, Phys.Lett. **B289**, 261 (1992)

- 33 A.Csótó, Phys.Rev. **C48**, 165 (1993)
- 34 W.-T.Chou, E.K.Warburton and B.A.Brown, Phys. Rev. **C47**, 163 (1993)
- 35 G.C.Li, I.Sick, R.R.Whitney and M.R.Yearian, Nucl.Phys. **A162**, 583 (1971)
- 36 J.C.Bergstrom, Nucl.Phys. **A262**, 196 (1976)
- 37 F.Figenbrod, Zeit.Phys. **228**, 337 (1969)
- 38 J.C.Bergstrom, U.Deutschmann and R.Neuhausen, Nucl.Phys. **A327**, 439 (1979)
- 39 F.Ajzenberg-Selove, Nucl.Phys. **A490**, 38 (1988)
- 40 V.I.Kukulin, V.T.Voronchev, T.D.Kaipov and R.A.Eramzhyan, Nucl.Phys. **A517**, 221 (1990)
- 41 A.Eskandarian, D.R.Lehman and W.C.Parke, Phys.Rev. **C38**, 2341 (1988)
- 42 J.C.Bergstrom, S.B.Kowalski and R.Neuhausen, Phys.Rev. **C25**, 1156 (1982)
- 43 V.Brudanin e.a., Nucl. Phys.**A587**, 557 (1995);  
V.Wiaux e.a., Abstract of PANIC-96, v.1, p.488,  
V.A.Kuzmin, A.A.Ovchinnikova and T.V.Tetereva, Yadernaya Fizika (Russian J. of Nucl.Phys.)  
**57**, 1954 (1994) and Izvestiya RAN (Physics) **59**, 163 (1995)
- 44 J.P.Deutsch e.a., Phys. Let. **26B**, 315 (1968)
- 45 R.Mach and S.S.Kamalov, Nucl. Phys. **A551**, 601 (1990)
- 46 R.A.Eramzhyan , M.Gmitro, S.S.Kamalov and R.Mach, J.Phys.G **14**, 1511 (1988);  
R.A.Eramzhyan, M.Gmitro and S.S.Kamalov, Phys. Rev. **C41**, 2865 (1990)
- 47 S.Ritt et. al., Phys.Rev **C52**, 2885 (1995)
- 48 S.Ritt et. al., Phys. Rev **C43**, 745 (1991)
- 49 K.Shoda, O.Sasaki and T.Kohmura, Phys.Lett. **101B**, 124 (1981)
- 50 J.Shaw, T.Kobayashi, W.Klayton, L.Ghedira, D.Myers, P.Stoler, P.K.Teng, E.J.Winhold,  
J.H.J.Distelbrink, Phys.Rev. **C43**, 1800 (1991)

- <sup>51</sup> K.Wildermuth and Th.Kannelopoulos, Nucl.Phys. **A7**, 150 (1958)
- <sup>52</sup> Yu.M.Tchuvil'sky, Izvestia Academy Nauk USSR, ser. fiz., **54**, 134 (1990)
- <sup>53</sup> Yu.F.Smirnov and Yu.M.Tchuvils'ky, J.Phys. **G4**, L1 (1978)
- <sup>54</sup> L.Ya.Glozman, V.G.Neudatchin and I.T.Obukhovsky, Phys.Rev. **C48**, 389 (1993)
- <sup>55</sup> M.L.Goldberger and S.B.Treiman, Phys.Rev. **110**, 1178 (1958)
- <sup>56</sup> I.Blomqvist and L.M.Laget, Nucl. Phys. **A280**, 405 (1977);  
J.M.Laget, Nucl.Phys. **A481**, 765 (1988)

TABLES

TABLE I. *Renormalization effects for some matrix elements in electron scattering on  ${}^6\text{Li}$ . A — for elastic scattering, B — for the transition to the  $J^\pi T = 3^+0$  level, C — for transition to the  $J^\pi T = 0^+1$  level*

		MDM		AMDM <sub>C</sub>		AMDM <sub>K</sub>	
		$q = 0.5\text{fm}^{-1}$	$q = 2.5\text{fm}^{-1}$	$q = 0.5\text{fm}^{-1}$	$q = 2.5\text{fm}^{-1}$	$q = 0.5\text{fm}^{-1}$	$q = 2.5\text{fm}^{-1}$
A	[000] <sub>0</sub>	.4669	6.290E-3	.4723	7.981E-3	.4657	5.261E-3
B	[022] <sub>0</sub>	3.825E-2	1.621E-2	3.375E-2	1.752E-2	3.888E-2	1.656E-2
C	[101] <sub>1</sub>	-.2004	4.235E-3	-.2081	1.081E-2	-.1954	8.840E-3
	[121] <sub>1</sub>	-3.839E-3	-5.728E-4	-4.016E-3	-8.531E-4	-4.152E-2	-7.007E-4
	[111p] <sub>1</sub> / $M_N$	-2.199E-3	-4.629E-4	-2.883E-3	-6.968E-4	-2.684E-3	-6.043E-4
	[011p] <sub>1</sub> / $M_N$	7.303E-3	-1.097E-3	7.731E-3	-1.939E-3	7.728E-3	-1.546E-3

TABLE II. *Static properties of six-nucleon nuclei*

Nucleus	$\langle r^2 \rangle_{ch}^{1/2}, \text{fm}$	$\mu/\mu_0$	$Q, \text{fm}^2$	$\langle r^2 \rangle_{body}^{1/2}, \text{fm}$	$r_{halo}, \text{fm}$
	${}^6\text{Li}$	${}^6\text{Li}$	${}^6\text{Li}$	${}^6\text{He}$	${}^6\text{He}$
MDM	2.55	0.829	0.49	2.43	0.74
AMDM <sub>C</sub>	2.48	0.838	0.49	2.33	
AMDM <sub>K</sub>	2.55	0.829	0.51	2.44	0.80
Exper.	2.56	0.822	-0.082	2.33±0.04	0.87±0.06 [32]

TABLE III. Amplitudes of muon capture in  ${}^6\text{Li}$ , their ratio and capture rates for three versions of the model. Numbers with \* are given for results obtained without the velocity terms.

	MDM	AMDM <sub>C</sub>	AMDM <sub>K</sub>
$\Delta T_1$	4.74E-3	2.47E-3	3.97E-3 1.56E-3*
$\Delta T_2$	-.136	-.139	-.147 0.031*
$T_1$	0.198	0.205	0.193
$T_2$	0.0687	0.0708	0.0660
$X$	-0.152	-0.159	-0.168
$\Lambda, \text{s}^{-1}$	1259	1351	1192 1225*
$\Lambda_+/\Lambda_-$	0.0417	0.0423	0.0431 0.0247*

## Figure captions

Fig.1. The Jacoby coordinates of the  $\alpha$ -2N system.

Fig.2. Longitudinal elastic form factor of  ${}^6\text{Li}$ . The solid line — calculation within the framework of the AMDM<sub>K</sub>, dashed line — within the AMDM<sub>C</sub> and dotted line — within the MDM. Experimental data from Ref. [35].

Fig.3. The square root of the reduced quadrupole transition strength  $B(C2,q)$  in units  $efm^2$  for transition to the  $J^\pi T = 3^+0$  level in  ${}^6\text{Li}$ . Experimental data from Refs. [36–38] The notations are as in Fig.2.

Fig.4. The form factor for transition to the  $J^\pi T = 3^+0$  level of  ${}^6\text{Li}$ . Open triangles are experimental data from Ref. [38], solid triangles are data from Ref. [35]. The notations are as in Fig.2.

Fig.5. Elastic magnetic form factor of  ${}^6\text{Li}$ . Experimental data from Ref. [42]. The notations are as in Fig.2.

Fig.6. Inelastic magnetic form factor for transition to the  $J^\pi T = 0^+1$  level of  ${}^6\text{Li}$ . Experimental data from Ref. [38]. The notations are as in Fig.2.

Fig.7. Muon capture rate for transition to the ground state of  ${}^6\text{He}$ . Experimental data from Ref. [44]. The notations are as in Fig.2.

Fig.8. Ratio of the hyperfine muon capture rates to the ground state of  ${}^6\text{He}$ . The notations are as in Fig.2.

Fig.9. The differential pion elastic cross section on  ${}^6\text{Li}$  at  $T_\pi = 134$  MeV. The second order pion-nucleus potential is omitted. The notations are as in Fig.2.

Fig.10. The differential inelastic pion cross section to the  $J^\pi T = 3^+0$  level at  $T_\pi = 134$  MeV. The second order pion-nucleus potential is omitted. The notations are as in Fig.2.

Fig.11. The vector analyzing power for pion elastic scattering on polarized  ${}^6\text{Li}$  at  $T_\pi = 134$  MeV. The second order pion-nucleus potential is omitted. The notations are as in Fig.2.

Fig.12. The vector analysing power for pion inelastic scattering to the  $J^\pi T = 3^+0$  level on polarized  ${}^6\text{Li}$  at  $T_\pi = 134$  MeV. The second order pion-nucleus potential is omitted. The notations

are as in Fig.2.

Fig.13. Experimental and calculated differential cross section for pion photoproduction on  ${}^6\text{Li}$  at  $T_\gamma = 200 \text{ MeV}$  with formation of  ${}^6\text{He}$  in its ground state for three versions of the model. The notations are as in Fig.2. Experimental data are from Refs. [49,50].

Fig.14. Calculated differential cross section for pion photoproduction on  ${}^6\text{Li}$  at  $T_\gamma = 320 \text{ MeV}$  with formation of  ${}^6\text{He}$  in its ground state for three versions of the model. The notations are as in Fig.2.

Fig.15. Calculated beam asymmetry for pion photoproduction on  ${}^6\text{Li}$  at  $T_\gamma = 320 \text{ MeV}$  with formation of  ${}^6\text{He}$  in its ground state for three versions of the model. The notations are as in Fig.2.

Fig.16. Calculated beam asymmetry for pion photoproduction on  ${}^6\text{Li}$  at  $T_\gamma = 320 \text{ MeV}$  with formation of  ${}^6\text{He}$  in its ground state for three values of  $\Delta$  — isobar mass in nucleus: solid line — the mass is equal to the mass of the free particle ( $M_\Delta$ ), short dashed line — the mass is larger by 5% than the free mass, long dashed line — the mass is smaller by 5% than the free mass. The calculation is within the framework of the AMDM<sub>K</sub>.

Fig.17. Calculated differential cross section for pion photoproduction on  ${}^6\text{Li}$  at  $T_\gamma = 320 \text{ MeV}$  with the formation of  ${}^6\text{He}$  in its ground state for three values of  $\Delta$  — isobar mass in nucleus: solid line — the mass is equal to the mass of the free particle ( $M_\Delta$ ), short dashed line — the mass is larger by 5% than the free mass, long dashed line — the mass is smaller by 5% than the free mass. The calculation is within the framework of the AMDM<sub>K</sub>.

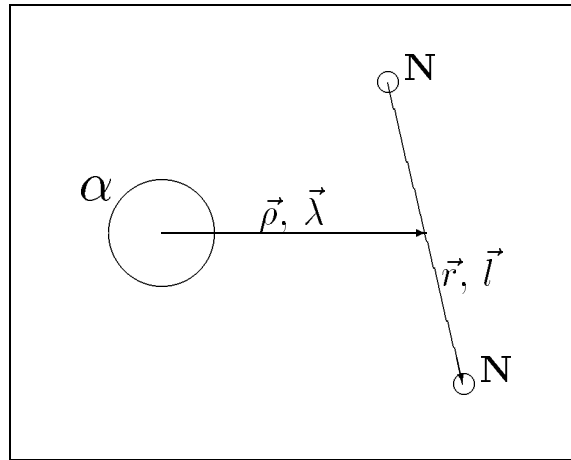


Fig.1 R.A.Eramzhyan et al.





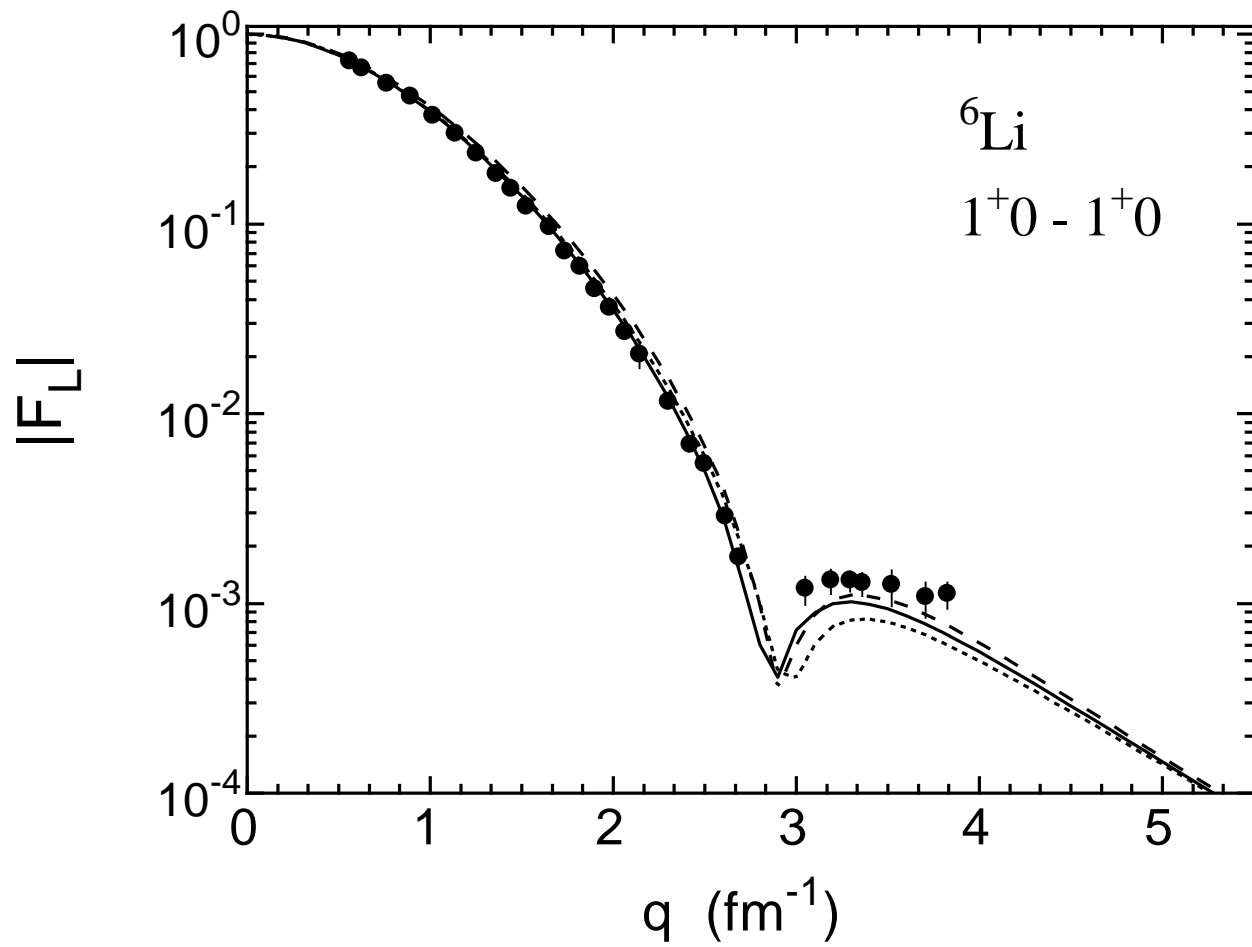


Fig.2 R.A.Eramzhyan et al.

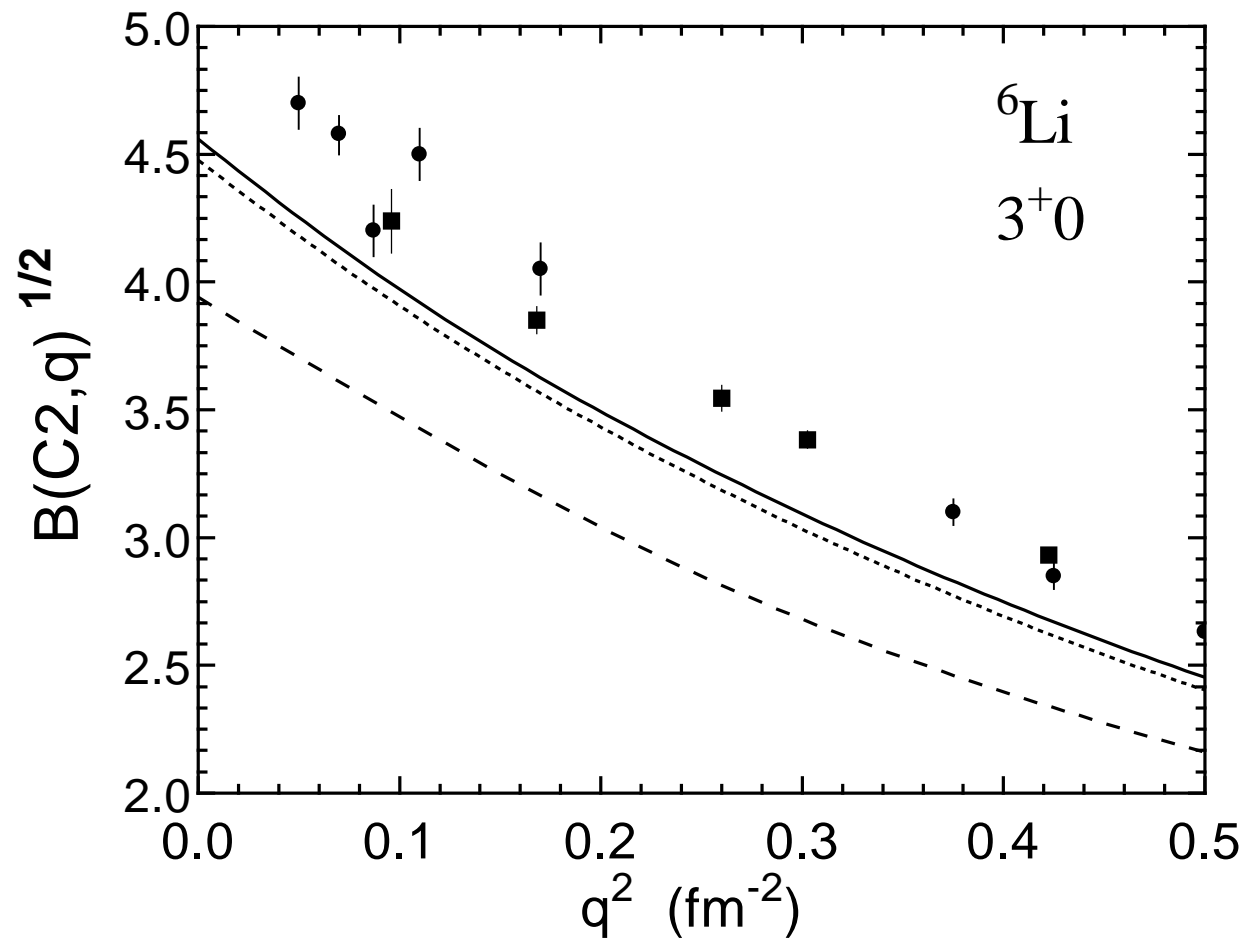


Fig.3 R.A.Eramzhyan et al.

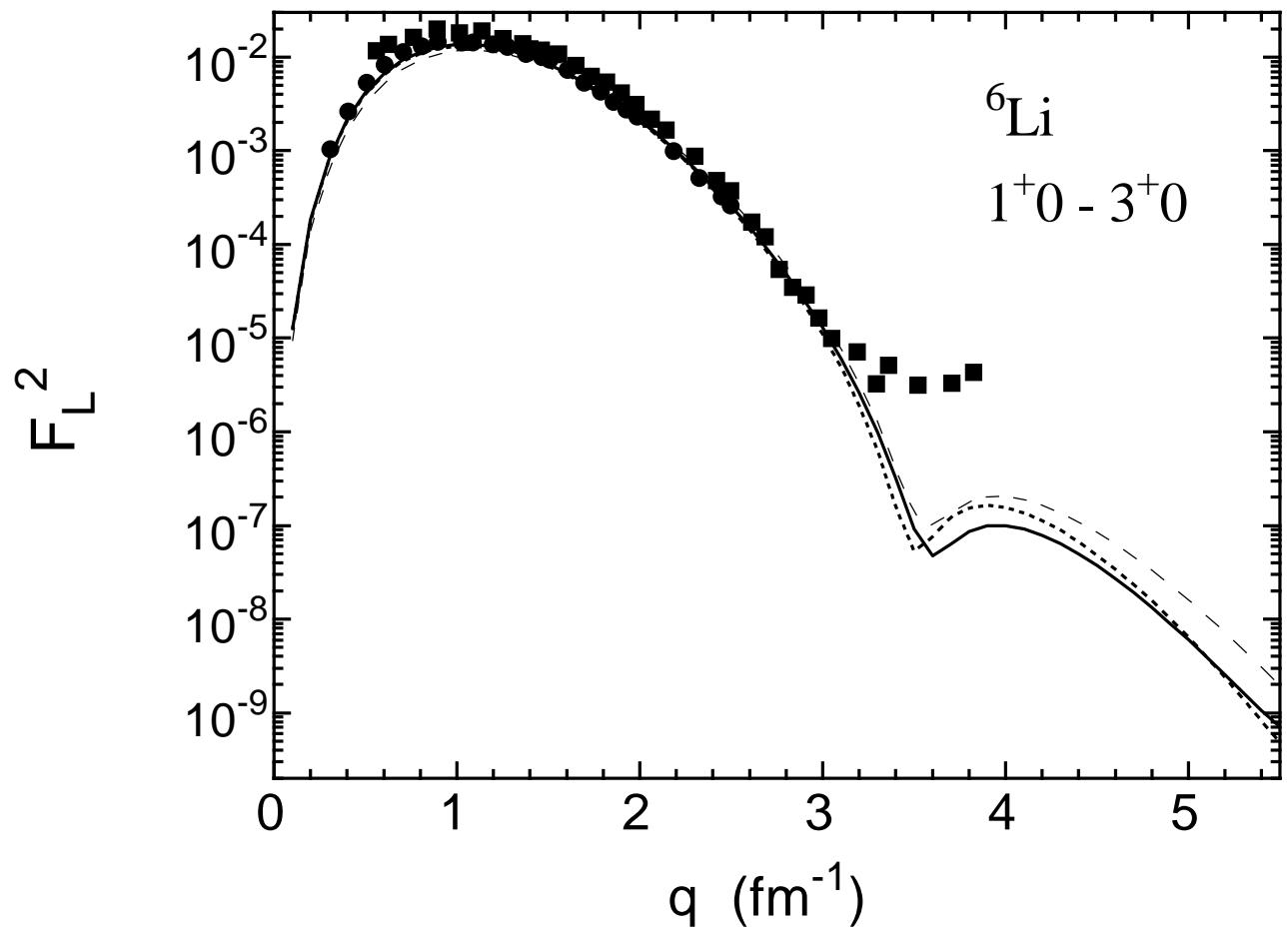


Fig.4 R.A.Eramzhyan et al.

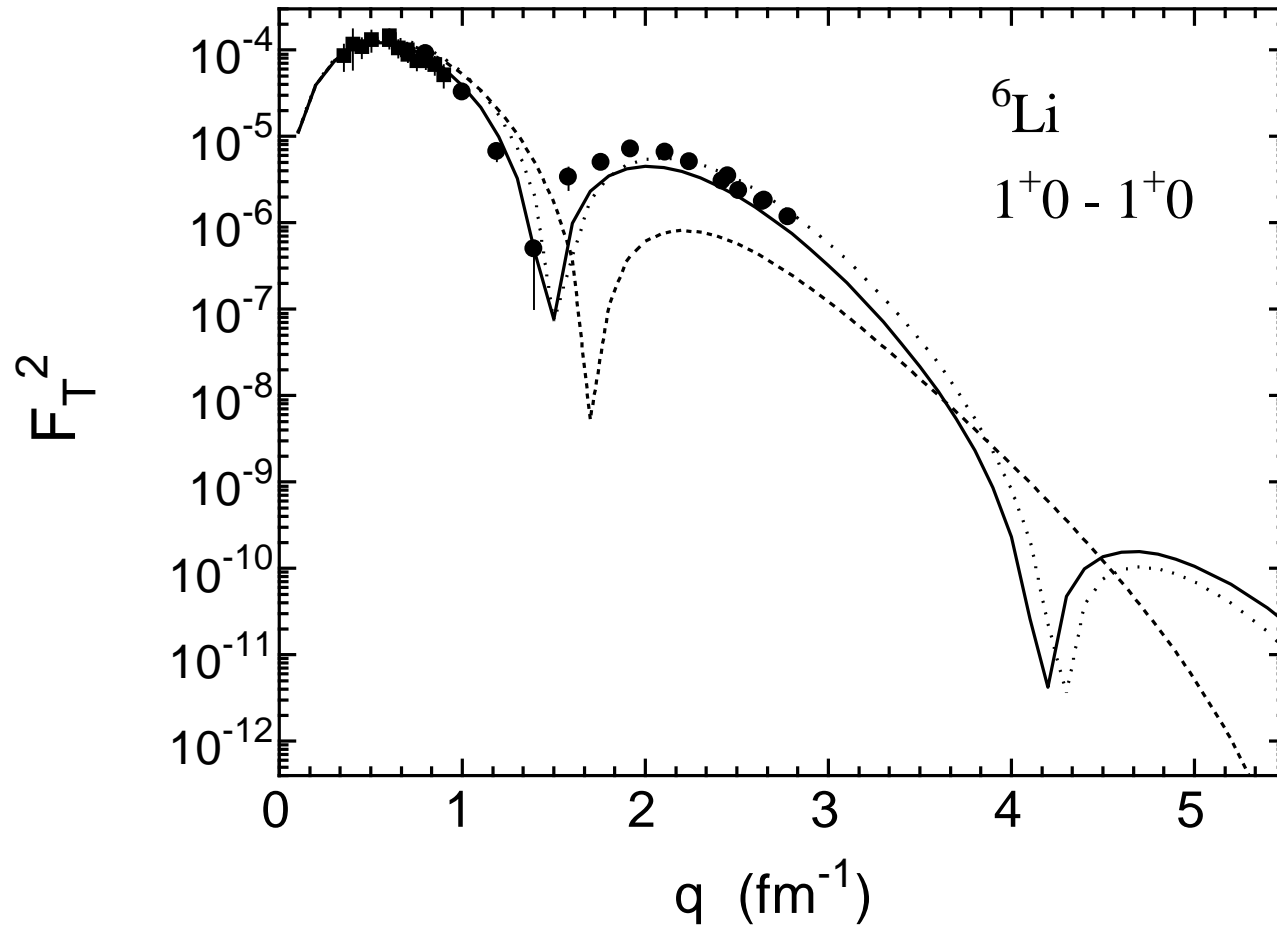


Fig.5 R.A.Eramzhyan et al.

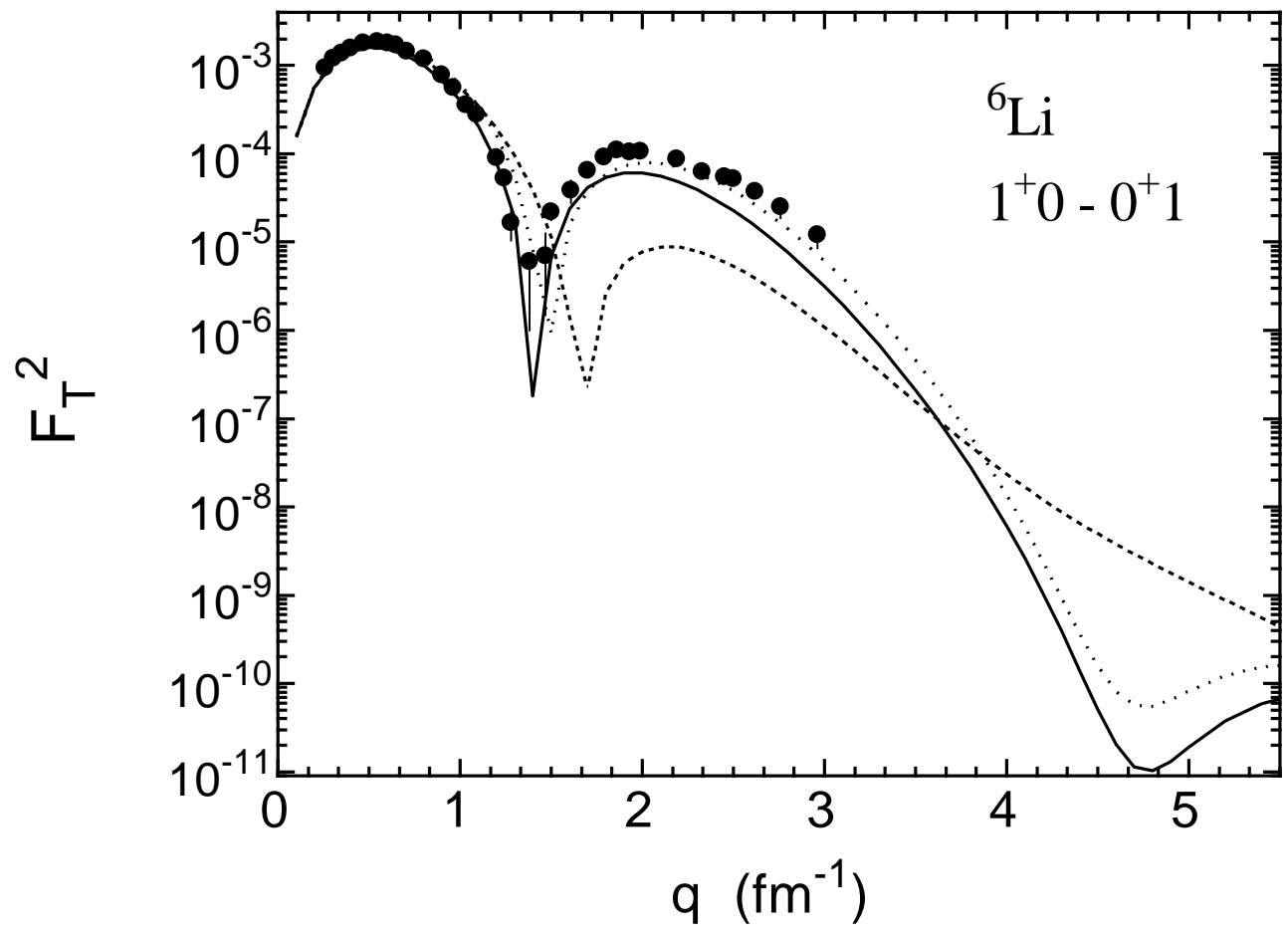


Fig.6 R.A.Eramzhyan et al.

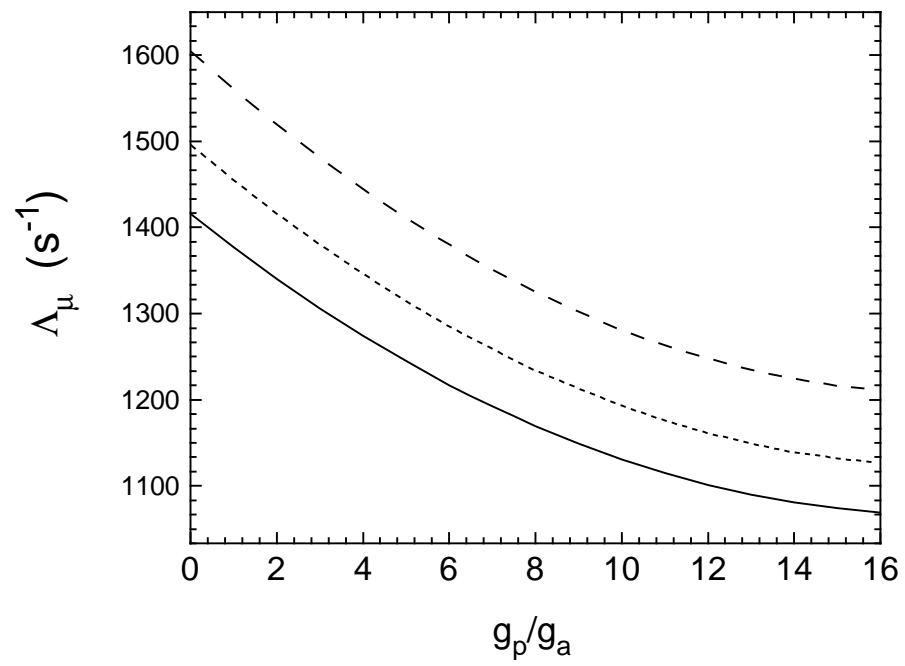


Fig.7 R.A.Eramzhyan et al.

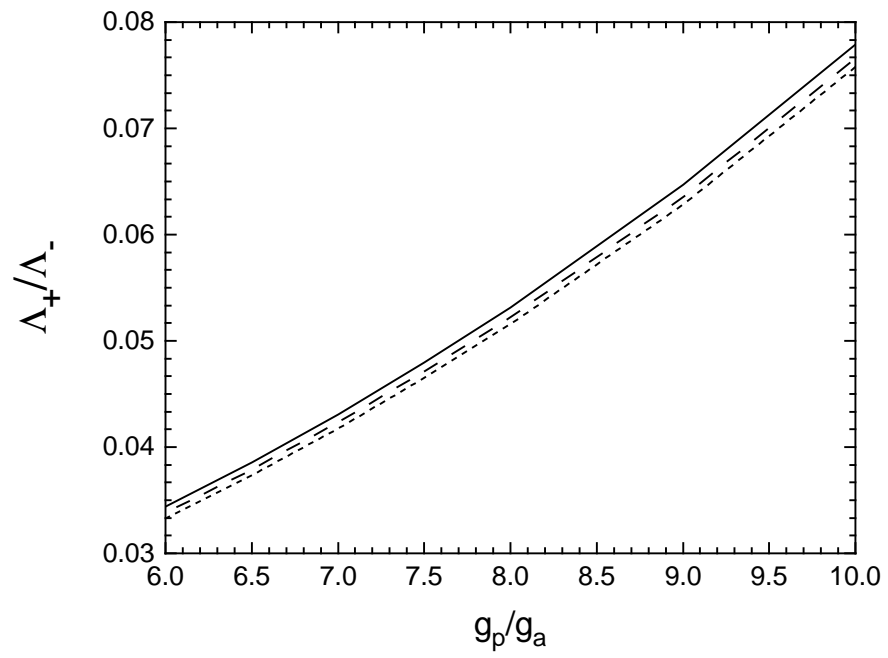


Fig.8 R.A.Eramzhyan et al.



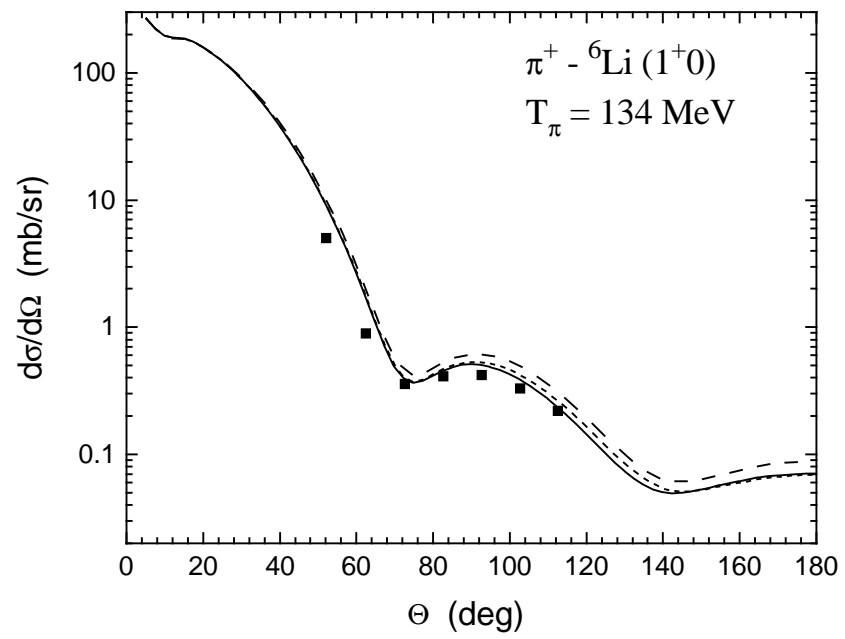


Fig.9 R.A.Eramzhyan et al.

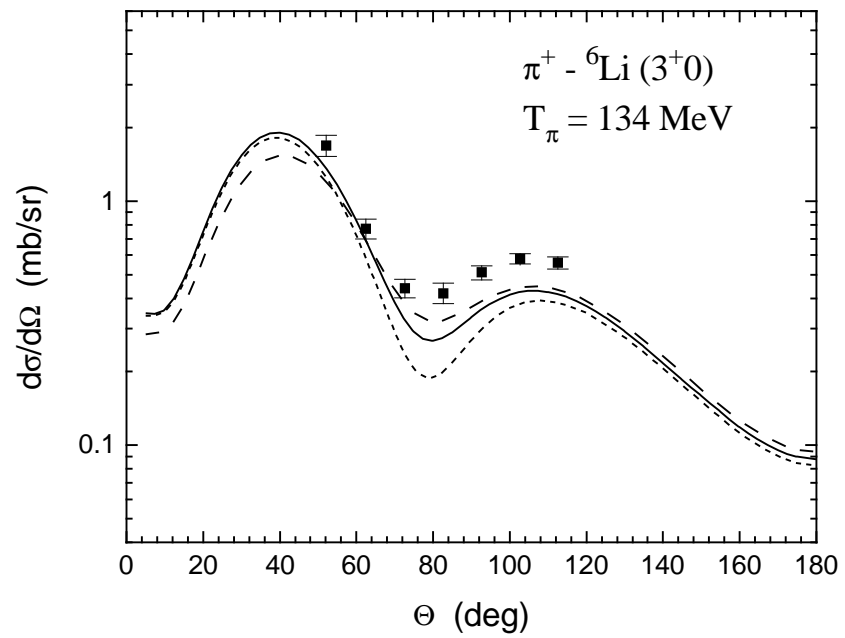


Fig.10 R.A.Eramzhyan et al.

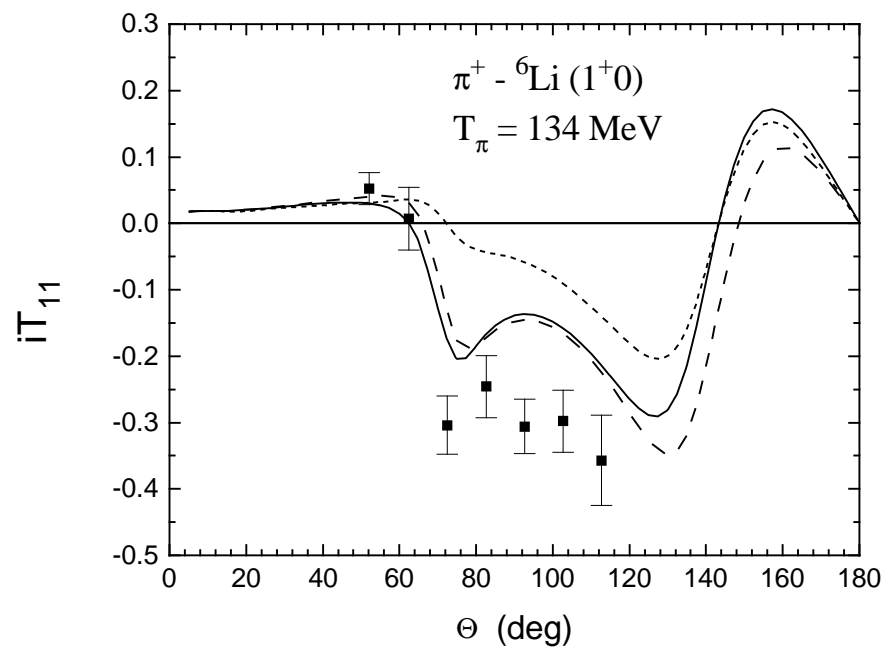


Fig.11 R.A.Eramzhyan et al.

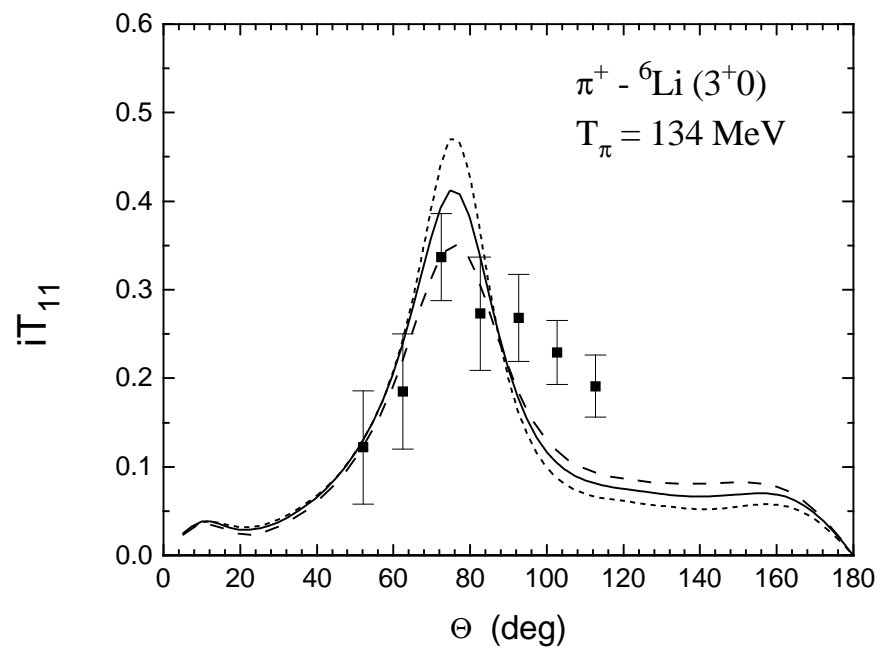


Fig.12 R.A.Eramzhyan et al.

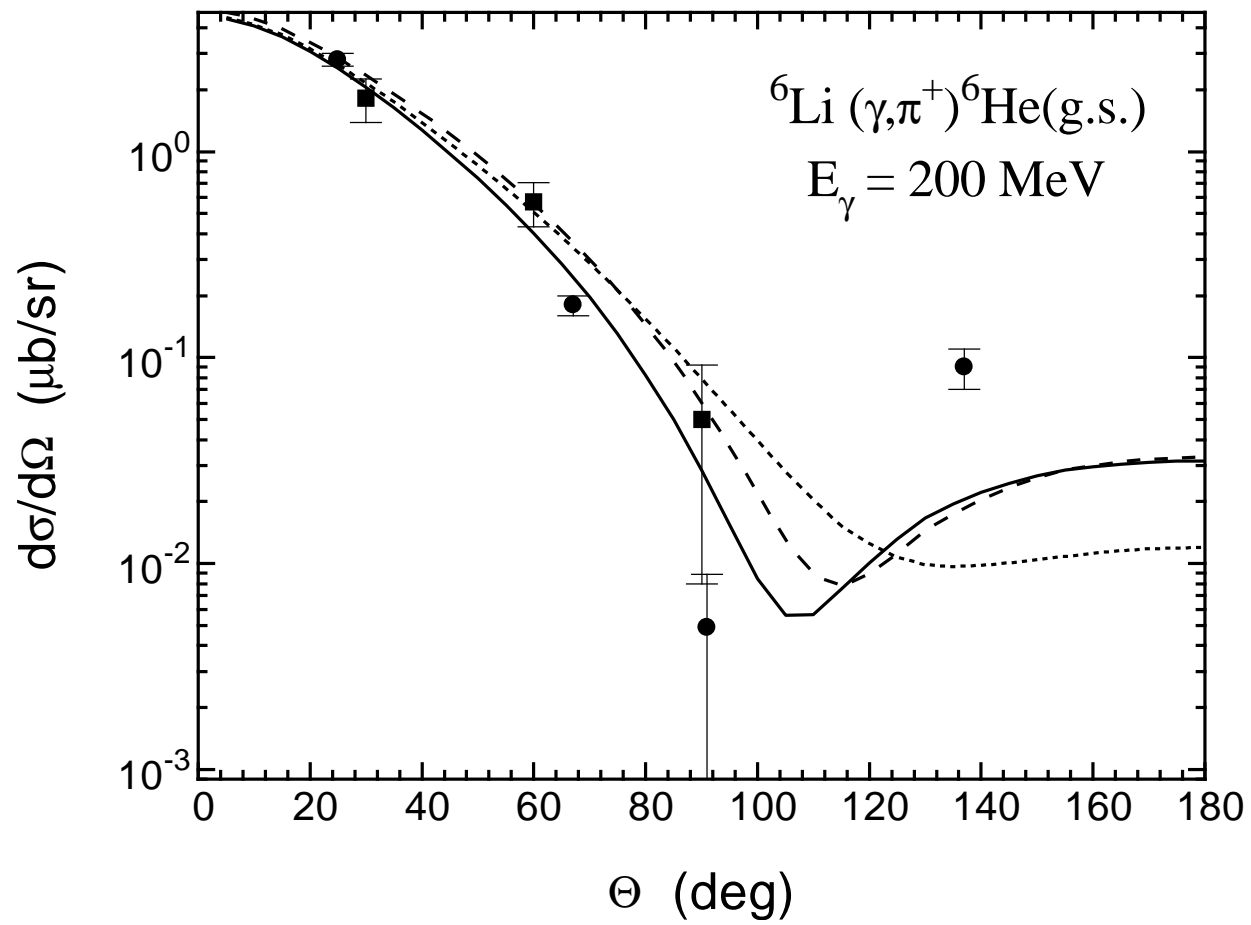


Fig.13 R.A.Eramzhyan et al.

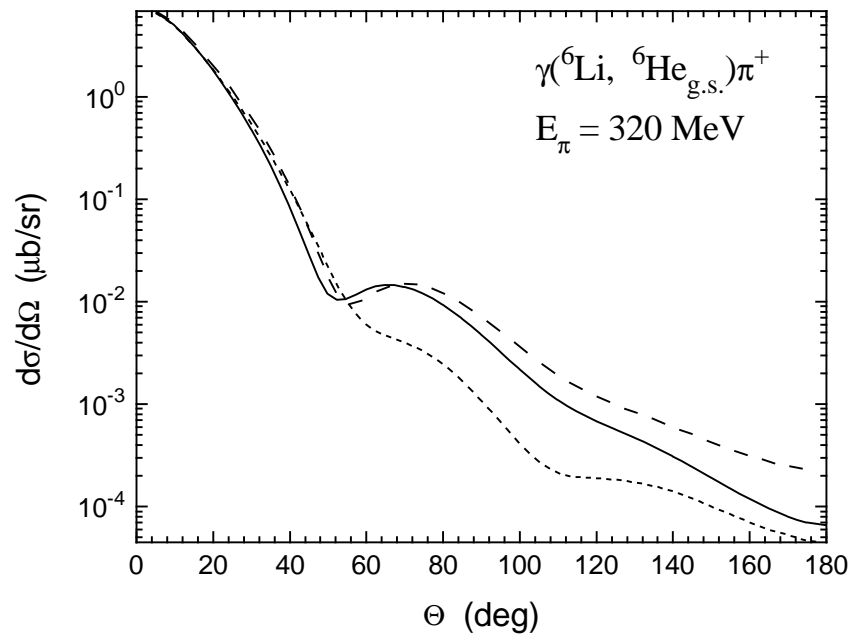


Fig.14 R.A.Eramzhyan et al.

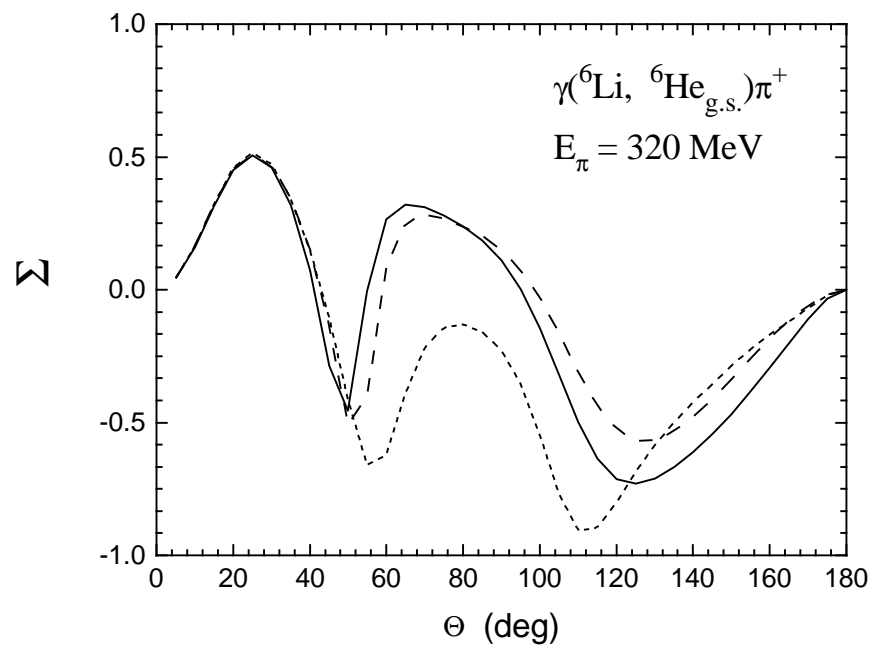


Fig.15 R.A.Eramzhyan et al.

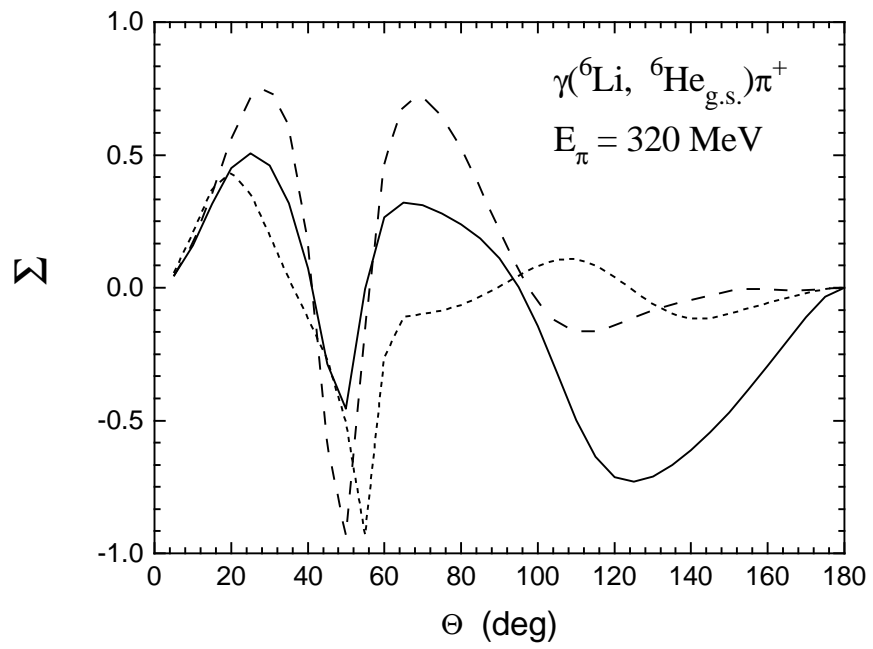


Fig.16 R.A.Eramzhyan et al.



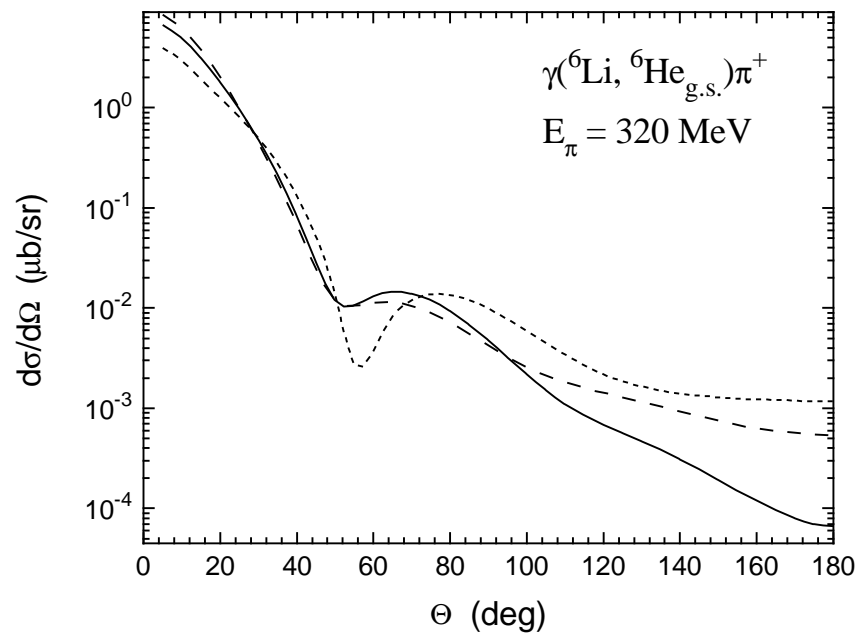


Fig.17 R.A.Eramzhyan et al.